

NoisyMix: Boosting Robustness by Combining Data Augmentations, Stability Training, and Noise Injections

N. Benjamin Erichson^{*1} Soon Hoe Lim^{*2} Francisco Utrera¹³ Winnie Xu⁴ Ziang Cao¹
Michael W. Mahoney³

Abstract

For many real-world applications, obtaining stable and robust statistical performance is more important than simply achieving state-of-the-art predictive test accuracy, and thus robustness of neural networks is an increasingly important topic. Relatedly, data augmentation schemes have been shown to improve robustness with respect to input perturbations and domain shifts. Motivated by this, we introduce *NoisyMix*, a training scheme that combines data augmentations with stability training and noise injections to improve both model robustness and in-domain accuracy. This combination promotes models that are consistently more robust and that provide well-calibrated estimates of class membership probabilities. We demonstrate the benefits of *NoisyMix* on a range of benchmark datasets, including ImageNet-C, ImageNet-R, and ImageNet-P. Moreover, we provide theory to understand implicit regularization and robustness of *NoisyMix*.

1. Introduction

While deep learning has achieved remarkable results in computer vision and natural language processing, much of the success is driven by improving test accuracy. However, it is well-known that deep learning models are typically brittle and sensitive to noisy and adversarial environments. This limits their applicability in a range of real-world problems, which require, at a minimum, that deep learning methods produce stable statistical predictions.

One can distinguish between structural stability (i.e., how sensitive is a model’s prediction to small perturbations of the weights, or model parameters) and input stability (i.e., how sensitive is a model’s prediction to small perturbations of the input data). Structural stability is particularly im-

portant when compression techniques (e.g., quantization) or different hardware systems introduce small errors to the model’s weights. Input stability is important when models (e.g., a vision model in a self-driving car) should operate reliably in noisy environments. Overall, robustness is an important topic within machine learning and deep learning, but the many facets of robustness prohibit the use of a single metric for measuring it (Hendrycks et al., 2021).

In this work, we are specifically interested in studying input stability (robustness) with respect to common data corruptions and domain shifts that naturally occur in many real-world applications. To do so, we use datasets such as ImageNet-C (Hendrycks & Dietterich, 2018) and ImageNet-R (Hendrycks et al., 2021). ImageNet-C provides examples to test the robustness of a model with respect to common corruptions, including noise sources such as white noise, weather variations such as snow, and digital distortions such as image compression. ImageNet-R provides examples to test robustness to naturally occurring domain shifts in form of abstract visual renditions, including graffiti, origami, or cartoons. State-of-the-art models often fail when facing such common corruptions and domain shifts. For instance, the predictive accuracy of a ResNet-50 (He et al., 2016b) trained on ImageNet drops by over 35%, when evaluated on ImageNet-C (Hendrycks & Dietterich, 2018).

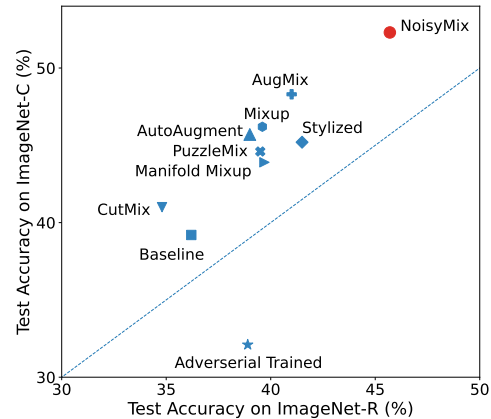


Figure 1: ResNet-50 models trained with data augmentation methods. *NoisyMix* considerably improves the test accuracy on ImageNet-C and ImageNet-R, indicating improved robustness to common corruptions and domain shifts.

^{*}Equal contribution ¹School of Engineering, University of Pittsburgh ²Nordita, KTH Royal Institute of Technology and Stockholm University ³ICSI and Department of Statistics, UC Berkeley ⁴Department of Computer Science, University of Toronto. Correspondence to: N. Benjamin Erichson <erichson@pitt.edu>, Soon Hoe Lim <soon.hoe.lim@su.se>.

Data augmentation methods such as *Mixup* (Zhang et al., 2018), *AutoAugment* (Cubuk et al., 2019), training on *stylized* ImageNet (Geirhos et al., 2018), and *AugMix* (Hendrycks et al., 2020) have the ability to improve the resilience to various data perturbations and domain shifts. Figure 1 shows the obtained test accuracies on ImageNet-C and ImageNet-R for ResNet-50 models trained with different augmentation schemes on ImageNet (see Sec. 4 for details). Indeed, it can be seen that data augmentation helps to achieve better test accuracies on these corrupted and domain-shifted test sets when compared to a “vanilla” trained model. Among these, our proposed method, *NoisyMix*, is the most effective in improving robustness. In contrast, adversarial training (Shafahi et al., 2019a) decreases robustness to common corruptions. The reason for this is that while adversarial training helps to improve robustness to perturbations that are manifested in the high-frequency domain, it reduces robustness to common corruptions that are often manifested in the low-frequency domain (Yin et al., 2019).

Contributions. We propose and study *NoisyMix*¹, an effective data augmentation strategy that combines stability training with data augmentations and noise injections to improve both robustness to common corruptions and in-domain test accuracy. In addition, *NoisyMix* promotes predictions that are well-calibrated. We show that, compared to AugMix, *NoisyMix* improves the robust accuracy on ImageNet-C and ImageNet-R by over 4%, while achieving comparable accuracy on the clean ImageNet validation set. Moreover, *NoisyMix* has comparable training costs to AugMix. We also show that *NoisyMix* achieves state-of-the-art performance on CIFAR-10-C and CIFAR-100-C, using preactivated ResNet-18 and Wide-ResNet-28x2 architectures.

Our empirical results suggest that the improved effects of *NoisyMix* come from implicit regularization. To understand this better, we illustrate these effects via toy experiments (see App. A) and provide theoretical results that identify the effects (see Theorem 1-2 in App. B). Importantly, we show that, under assumptions similar to those made in (Lamb et al., 2019; Lim et al., 2021b), minimizing the *NoisyMix* loss corresponds to minimizing an upper bound on the sum of an adversarial loss, a stability objective, and data-dependent regularizers (see Theorem 3 in App. C). This suggests that *NoisyMix* provides an inductive bias towards improving model robustness with respect to both adversarial perturbations and common corruptions, when compared to standard training.

Notation. $[K] := \{1, \dots, K\}$, \odot denotes Hadamard product, $\mathbf{1}$ denotes the vector with all components equal one. For a vector v , $\|v\|_p$ denotes its l_p norm for $p > 0$. $M_\lambda(a, b) := \lambda a + (1 - \lambda)b$, for random variables a, b, λ .

¹Research codes are shared via <https://github.com/erichson/NoisyMix>.

2. Related Work

The study of stability of modelling methods for real-world phenomena has a long history and is central in statistics, numerical analysis, and dynamical systems (Yu, 2013). In this work, we are mainly concerned with improving input stability of deep neural networks for computer vision tasks. In particular, there are two types of input perturbations that have recently led to a surge of interest: (i) adversarial perturbations, and (ii) common corruptions. The class of adversarial perturbations consists of artificially crafted perturbations specifically designed to fool neural networks while being imperceptible for the human eye (Szegedy et al., 2013; Goodfellow et al., 2014). Common corruptions are a class of perturbations that naturally occur in real-world applications (Hendrycks & Dietterich, 2018), and are often more relevant in real-world science and engineering applications than adversarial perturbations (Rusak et al., 2020).

Early work by Dodge & Karam (2016) has revealed how sensitive neural networks (trained on high quality images) are to slight degradation of image quality and common corruptions. Hendrycks & Dietterich (2018) introduced a more extensive benchmark dataset for testing robustness on a comprehensive set of common corruptions with varying intensity levels. Subsequently, it has been shown that data augmentation and noise injection schemes can help to improve robustness (Yin et al., 2019) to common corruptions.

As an alternative, Hendrycks et al. (2019) and Xie et al. (2020) showed that pretraining on larger and more diverse datasets (e.g., JFT-300M (Hinton et al., 2015)) can help to improve robustness, but Hendrycks et al. (2021) showed that these strategies do not consistently do better if a broader range of distribution shifts is considered. The disadvantages of pretraining on larger datasets are the increased computational costs and the limited availability of massive computer vision datasets. Hence, we limit our discussion in this paper to data augmentation and noise injection strategies that can be applied to standard architectures trained on common computer vision benchmark datasets (e.g., ImageNet).

Most relevant for our work are data augmentation methods that aim to reduce the generalization error and improve robustness by introducing implicit regularization (Mahoney, 2012; Kukačka et al., 2017) into the training process. By data augmentation, we refer to schemes that do not introduce new data but train a model with virtual training examples (e.g., proper transformations of the original data) in the vicinity of a given training dataset. Basic examples are random cropping and horizontal flipping of input images (Krizhevsky et al., 2012).

Mixup (Zhang et al., 2018) is a popular data augmentation method, which creates new training examples by forming linear interpolations between random pairs of examples and

their corresponding labels. Despite its simplicity it is an extremely efficient scheme and helps to improve generalization and robustness of models with minimal computation overhead. Motivated by Mixup, a range of other innovations have been proposed subsequently. Manifold Mixup (Verma et al., 2019) extends the idea of interpolating between data points in input space to hidden representations, leading to models that have smoother decision boundaries. Noisy Feature Mixup (Lim et al., 2021b) generalizes the idea of both Mixup and Manifold Mixup by taking linear combinations of pairs of perturbed input and hidden representations.

Another approach involves zeroing out parts of an input image (DeVries & Taylor, 2017) to prevent a model from focusing on a limited image region. CutMix (Yun et al., 2019) extends this idea by replacing the removed parts with a patch from another image. PuzzleMix (Kim et al., 2020) is a mixup method that further improves CutMix by leveraging saliency information and local statistics of the original input data to decide how to mix two data points.

Geirhos et al. (2018) proposed to train models on a stylized version of ImageNet, which helps to increase shape bias and in turn improves robustness to common corruptions. To do so, they use a style transfer network that applies artwork styles to images that are then used to train the model. Similar good results are achieved by AutoAugment (Cubuk et al., 2019), a method that automatically searches for improved data augmentation policies.

AugMix (Hendrycks et al., 2020) is designed to improve robustness to common corruptions, which is achieved by leveraging a diverse set of basic data augmentations (e.g., translate, posterize, solarize) and applying consistency regularization (using the Jensen-Shannon divergence loss). This approach significantly improves robustness when compared to the previously discussed data augmentation methods.

Noise injections are another form of data augmentations, which introduce regularization into the training process (Bishop, 1995). Most commonly, the models are trained with noise perturbed inputs (An, 1996). Noise can also be injected into the activation functions (Gulcehre et al., 2016), or the hidden layers of a neural network (Camuto et al., 2020; Lim et al., 2021b). Recently, Rusak et al. (2020) has demonstrated that training a model with various noise types helps to improve robustness to unseen common corruptions.

3. Method

NoisyMix implements feature mixup and noise injections (Lim et al., 2021b) on top of a stability training scheme (Zheng et al., 2016) on an augmented data set (Hendrycks et al., 2020) in a single setup to boost both accuracy and robustness. While components underlying *NoisyMix* exist in the literature, the devil is in the details to get the

method right, so we motivate and describe the procedures of *NoisyMix* for multi-class classification in the following.

3.1. Components of *NoisyMix*

Data Augmentation. First, we augment the clean data with appropriately transformed data, obtained by applying the operations used in AugMix to the clean data. The transformed data are highly diverse because the operations are sampled stochastically and then layered on the same input image. Such diverse transformations are crucial for enabling model robustness by discouraging the model from memorizing fixed augmentations (Hendrycks et al., 2020).

Stability Training. Second, we consider a stability training scheme on the augmented training data (Zheng et al., 2016). Stability training stabilizes the output of a model against small perturbations to input data, thereby enforcing robustness. Since the classifiers are probabilistic in nature, we consider a probabilistic notion of robustness, which amounts to making them locally Lipschitz with respect to some distance on the input and output space. This ensures that a small perturbation in the input will not lead to large changes (as measured by some statistical distance) in the output.

We now formalize a notion of robustness. Let $p > 0$. We say that a model $f : \mathcal{X} \rightarrow \mathcal{Y}$ is α_p -robust if for any $(x, y) \sim \mathcal{D}$ such that $f(x) = y$, one has, for any data perturbation $\delta x \in \mathcal{X}$,

$$\|\delta x\|_p \leq \alpha_p \implies f(x) = f(x + \delta x).$$

An analogous definition can be given for distribution-valued outputs, which leads to a notion of probabilistic robustness. Let D be a metric or divergence between two probability distributions. We say that a model $F : \mathcal{X} \rightarrow \mathcal{P}(\mathcal{Y})$, i.e., the space of probability distributions on \mathcal{Y} , is (α_p, ϵ) -robust with respect to D if, for any $x, \delta x \in \mathcal{X}$,

$$\|\delta x\|_p \leq \alpha_p \implies D(F(x), F(x + \delta x)) \leq \epsilon.$$

In practice, stability training involves formulating a loss that aims to flatten the model output in a small neighborhood of any input data, forcing the output to be similar between the original and perturbed copy. This is done by combining the standard cross-entropy loss with a suitable stability objective, encouraging model prediction to be more constant around the input data while mitigating underfitting.

Applying Noise Injections and Feature Mixup. To improve the robustness further, we judiciously combine the stability training scheme with mixup and noise injections at the level of input and hidden layers. The latter approach, Noisy Feature Mixup (NFM) (Lim et al., 2021b), generalizes input mixup (Zhang et al., 2018) and Manifold Mixup (Verma et al., 2019) in the sense that noise is injected when taking convex combinations of pairs of input and hidden

layer features. It has been shown that this makes the decision boundary smoother and helps improving robustness when predicting on out of distribution data (Lim et al., 2021b).

3.2. Formulation of NoisyMix

We consider multi-class classification with K labels. Denote the input space by $\mathcal{X} \subset \mathbb{R}^d$ and the output space by $\mathcal{Y} := \Delta^{K-1}$, where Δ^{K-1} is the probability simplex, i.e., a categorical distribution over K classes. The classifier, g , is constructed from a learnable deep neural network map $p : \mathcal{X} \rightarrow \Delta^{K-1}$, mapping an input x to its label, $g(x) = \arg \max_k p^k(x) \in [K]$. We are given a training set, $\mathcal{Z}_n := \{(x_i, y_i)\}_{i \in [n]} \cup \{(A(x_i), y_i)\}_{i \in [n]}$, consisting of $2n$ pairs of input and one-hot label, with each training pair $z_i := (x_i, y_i)$, $z_{ami} := (A(x_i), y_i) \in \mathcal{X} \times \mathcal{Y}$. The training pairs (x_i, y_i) are drawn independently from a ground-truth distribution $\mathcal{D} := \mathcal{D}_x \times \mathcal{D}_y$. Here, A denotes the random perturbation of an input, i.e., the *AugmentAndMix* function in (Hendrycks et al., 2020). In the sequel, we denote $\mathcal{A}(x)$ as the underlying conditional (on x) distribution from which the $A(x)$ is sampled from.

More precisely, for an (original) input x , we construct a virtual data point x_{am} as

$$A(x) = mx + (1 - m) \sum_{i=1}^3 w_i C(x) \sim \mathcal{A}(x), \quad (1)$$

where $m \sim \text{Beta}(\alpha, \alpha)$, the $w_i \sim \text{Dirichlet}(\alpha, \dots, \alpha)$ (with $\alpha := 1$), and C uniformly drawn from a set of operations whose elements including compositions of transformations such as rotating, translating, autocontrasting, equalizing, posterizing, solarizing, and shearing. They can be viewed as randomly perturbed input data, i.e., $A(x) = x + \delta x$, where the random perturbation $\delta x := (1 - m) \left(\sum_{i=1}^3 w_i C(x) - x \right)$ is additive and data-dependent.

Within this setting, we consider the expected *NoisyMix* loss:

$$L^{\text{NoisyMix}} = L^{\text{NFM}} + \gamma L^{\text{stability}}, \quad (2)$$

where $\gamma \geq 0$. This loss is a sum of two components: the expected NFM loss (Lim et al., 2021b) and an expected stability loss (Zheng et al., 2016). As in (Lim et al., 2021b), the expected NFM loss is given by:

$$L^{\text{NFM}} = \mathbb{E}_{(x,y),(x',y') \sim \mathcal{D}} \mathbb{E}_{\lambda \sim \text{Beta}(\alpha,\beta)} \mathbb{E}_{\xi \sim \mathcal{Q}} [l(p(M_{\lambda,\xi}(x, x')), M_{\lambda}(y, y'))],$$

for some loss function (e.g., cross-entropy) $l : \Delta^{K-1} \times \Delta^{K-1} \rightarrow [0, \infty)$ (note that the dependence of both l and p on the learnable parameter θ is suppressed in the notation), $\xi := (\xi^{\text{add}}, \xi^{\text{mult}})$ are drawn from some probability distribution \mathcal{Q} with finite first two moments, and

$$M_{\lambda,\xi}(x, x') = (\mathbb{1} + \sigma_1 \xi^{\text{mult}}) \odot M_{\lambda}(x, x') + \sigma_2 \xi^{\text{add}},$$

where σ_1 and σ_2 are tuning parameters.

We choose the distance measure D in the expected stability loss to be the Jensen-Shannon divergence (JSD) and minimize the deviation between the distribution on the clean input data and that on the transformed input data, i.e., we minimize $L^{\text{stability}} := L^{\text{JSD}}$, given by:

$$\mathbb{E}_{x,x' \sim \mathcal{D}_x} \mathbb{E}_{x_{am} \sim \mathcal{A}(x), x'_{am} \sim \mathcal{A}(x')} \mathbb{E}_{\lambda \sim \text{Beta}(\alpha,\beta)} \mathbb{E}_{\xi \sim \mathcal{Q}} JS_{\pi}(p(M_{\lambda,\xi}(x, x')), p(M_{\lambda,\xi}(x_{am}, x'_{am}))),$$

where JS_{π} denotes Jensen-Shannon divergence with the weights π , defined as follows: for $p_1, p_2 \in \Delta^{K-1}$ with the corresponding weights $\pi := (\pi_1, \pi_2) \in \Delta$, the JSD (Lin, 1991) between p_1 and p_2 is

$$JS_{\pi}(p_1, p_2) := H(\pi_1 p_1 + \pi_2 p_2) - \pi_1 H(p_1) - \pi_2 H(p_2),$$

with H the Shannon entropy, defined as $H(p) := -\sum_{k=1}^K p_k \ln(p_k)$ for $p \in \Delta^{K-1}$. Alternatively, $JS_{\pi}(p_1, p_2) = \pi_1 KL(p_1 \| \pi_1 p_1 + \pi_2 p_2) + \pi_2 KL(p_2 \| \pi_1 p_1 + \pi_2 p_2)$, where KL denotes the Kullback-Leibler divergence.

JSD measures the similarity between two probability distributions, and its square root is a true metric between distributions. Unlike the KL divergence and cross-entropy, it is symmetric, bounded, and does not require absolute continuity of the involved probability distributions. Similar to the KL divergence, $JS_{\pi}(p_1, p_2) \geq 0$, with equality if and only if $p_1 = p_2$. This follows from applying Jensen's inequality to the concave Shannon entropy. Moreover, JSD can interpolate between cross-entropy and mean absolute error for $\pi_1 \in (0, 1)$ (see Proposition 1 in (Engleson & Azizpour, 2021)). In GANs, JSD is used as a measure to quantify the similarity between the generative data distribution and the real data distribution (Goodfellow et al., 2020; Weng, 2019). We refer to (Lin, 1991; Engleson & Azizpour, 2021) for more properties of JSD. Note that, unlike L^{NFM} , L^{JSD} is computed without the use of the labels.

3.3. Theoretical Results

NoisyMix seeks to minimize a stochastic approximation of L^{NoisyMix} by sampling a finite number of $\lambda, \xi, x_{am}, x'_{am}$ values and using minibatch gradient descent to minimize this loss approximation. The empirical loss to be minimized during the training is

$$L_n^{\text{NoisyMix}} = \frac{1}{n^2} \sum_{i=1}^n \sum_{j=1}^n \mathbb{E}_{\lambda \sim \text{Beta}(\alpha,\beta)} \mathbb{E}_{\xi \sim \mathcal{Q}} [a_{i,j} + \gamma b_{i,j}],$$

where

$$a_{i,j} := l(p(M_{\lambda,\xi}(x_i, x_j)), M_{\lambda}(y_i, y_j)), \\ b_{i,j} := JS_{\pi}(p(M_{\lambda,\xi}(x_i, x_j)), p(M_{\lambda,\xi}(A(x_i), A(x_j)))).$$

In App. A, we illustrate the effectiveness of *NoisyMix* in smoothing the decision boundary for a binary classification task. Overall, we observe that *NoisyMix* leads to the smoothest decision boundary when compared to other methods (see Fig. 4), and thus more robust models, since the predicted label stays the same even if the data are perturbed.

To understand these regularizing effects of *NoisyMix* better, we provide some mathematical analysis via the lens of implicit regularization (Mahoney, 2012) in App. B (see Theorem 1 and Theorem 2). Such lens was adopted to understand stochastic optimization (Ali et al., 2020; Smith et al., 2021) and regularizing effects of noise injections (Camuto et al., 2020; Lim et al., 2021a; Gong et al., 2021). One common approach to study implicit regularization is to approximate it by an appropriate explicit regularizer, which we follow here for the regime of small mixing coefficient and noise levels. Importantly, in this regime, we also show that *NoisyMix* can lead to models with enhanced robustness and stability, as demonstrated by the following informal version of our main result (see Theorem 3).

Theorem (Informal). Let $\epsilon > 0$ be a small parameter, and rescale $1 - \lambda \mapsto \epsilon(1 - \lambda)$, $\sigma_{add} \mapsto \epsilon\sigma_{add}$, $\sigma_{mult} \mapsto \epsilon\sigma_{mult}$. Then, under certain simplifying assumptions,

$$L_n^{NoisyMix} \geq \frac{1}{n} \sum_{i=1}^n \max_{\|\delta_i\|_2 \leq \epsilon_i^{mix}} l(p(x_i + \delta_i), y_i) + \gamma \tilde{L}_n^{JSD} + \epsilon^2 L_n^{reg} + \epsilon^2 \phi(\epsilon), \quad (3)$$

for some data-dependent radii $\epsilon_i^{mix} > 0$, stability objective \tilde{L}_n^{JSD} , data-dependent regularizer L_n^{reg} , and function ϕ such that $\lim_{\epsilon \rightarrow 0} \phi(\epsilon) = 0$.

This theorem implies that minimizing the *NoisyMix* loss results in a small *regularized* adversarial loss and a stable model. Therefore, training with *NoisyMix* not only enhances robustness with respect to input perturbations, but it also imposes additional smoothness.

Lastly, we remark that one could generalize the JSD, which is designed for only two distributions, to provide a similarity measure for any finite number of distributions. This leads to the following definition (Lin, 1991):

$$JS_\pi(p_1, \dots, p_K) := H\left(\sum_{k=1}^K \pi_k p_k\right) - \sum_{k=1}^K \pi_k H(p_k) \\ = \sum_{k=1}^K \pi_k KL\left(p_k \parallel \sum_{j=1}^K \pi_j p_j\right),$$

where p_1, \dots, p_K are K probability distributions with weights $\pi := (\pi_1, \dots, \pi_K)$. We note that such a measure, with $K := 3$ and the $\pi_i := 1/3$, will be used in our experiments and was also used in (Hendrycks et al., 2020) for obtaining optimal results.

4. Experimental Results

4.1. Experiment Details

Datasets. We center our experiments around several recently introduced datasets to benchmark the robustness of neural networks to common corruptions and perturbations.

The ImageNet-C, CIFAR-10-C, and CIFAR-100-C datasets (Hendrycks & Dietterich, 2018) provide various corrupted versions of the original ImageNet (Deng et al., 2009) and CIFAR (Krizhevsky, 2009) test sets. Specifically, each dataset emulates noise, blur, weather, and digital distortions. In total, there are 15 different perturbation and corruption types, and for each type, there are sets with 5 severity levels which allows us to study the performance with respect to increasing data shifts. Figure 6 in the App. illustrates the different corruption types. The average accuracy across all corruption types and severity levels provides a score for robustness.

We also consider the ImageNet-R dataset (Hendrycks et al., 2021), which is designed to measure the robustness of models to various abstract visual renditions (e.g., graffiti, origami, cartoons). This dataset provides 30,000 image renditions for a subset of 200 ImageNet object classes. The collected renditions have textures and local image statistics that are distinct from the standard ImageNet examples. This dataset provides a test for robustness to naturally occurring domain shifts, and it is complementary to ImageNet-C, which is used to test robustness to synthetic domain shifts.

In addition, we consider the ImageNet-P dataset (Hendrycks & Dietterich, 2018), which provides 10 different perturbed sequences for each ImageNet validation image. Each sequence contains 30 or more frames, where each subsequent frame is a perturbed version of the previous frame. The applied perturbations are relatively subtle, ensuring that the frames do not go too far out-of-distribution. This dataset is specifically designed to evaluate the prediction stability of a model f , using the flip probability as a metric to evaluate stability. Specifically, the flip probability is computed as $FB_p = \frac{1}{m(n-1)} \sum_{i=1}^m \sum_{j=2}^n I(f(x_j^{(i)}) \neq f(x_{j-1}^{(i)}))$, for given m sequences $\{(x_i^{(i)}, \dots, x_n^{(i)})\}_{i=1}^m$ of length n for a corruption type p . Here I denotes an indicator function. Unstable models are characterized by a high flip probability, i.e., the prediction behavior across consecutive frames is erratic, whereas consistent predictions indicate stable statistical predictions. For sequences that are constructed with noise perturbations (i.e., white, shot and impulse noise), the following modified flip probability is computed: $FB_p = \frac{1}{m(n-1)} \sum_{i=1}^m \sum_{j=2}^n I(f(x_j^{(i)}) \neq f(x_i^{(i)}))$, which accounts for the fact that these sequences are not temporally related. We obtain a flip rate by dividing the flip probability of a given model with the flip probability of AlexNet (Hendrycks & Dietterich, 2018). Finally, the flip

Table 1: Clean test accuracy of ResNet-50 models on ImageNet, and average robust accuracy on ImageNet-C and ImageNet-R (higher values are better). In addition, we show the mean flip rate for ImageNet-P (lower values are better) and the robustness to adversarial examples constructed with FGSM (higher values are better). The values in parenthesis are the average robust accuracy for ImageNet-C and mean flip probability for ImageNet-P excluding noise perturbations.

	ImageNet ($\uparrow\%$)	ImageNet-C ($\uparrow\%$)	ImageNet-R ($\uparrow\%$)	ImageNet-P ($\downarrow\%$)	FGSM ($\uparrow\%$)
Baseline (He et al., 2016a)	76.1	39.2 (42.3)	36.2	58.0 (57.8)	6.6
Adversarial Trained (Salman et al., 2020)	63.9	32.1 (35.4)	38.9	33.3 (33.4)	43.1
Stylized ImageNet (Geirhos et al., 2018)	74.9	45.2 (46.6)	41.5	54.4 (55.2)	7.8
AutoAugment (Cubuk et al., 2019)	77.6	45.7 (47.3)	39.0	56.5 (57.7)	9.9
Mixup (Zhang et al., 2018)	77.5	46.2 (48.4)	39.6	56.4 (58.7)	23.5
Manifold Mixup (Verma et al., 2019)	76.7	43.9 (46.5)	39.7	56.0 (58.2)	27.7
CutMix (Yun et al., 2019)	78.6	41.0 (43.1)	34.8	58.6 (59.9)	33.7
Puzzle Mix (Kim et al., 2020)	78.7	44.6 (46.4)	39.5	55.5 (57.0)	28.4
AugMix (Hendrycks et al., 2020)	77.5	48.3 (50.5)	41.0	37.6 (37.2)	9.9
NoisyMix (ours)	77.6	52.3 (52.4)	45.7	28.5 (29.7)	29.6

rate is averaged across all corruption types to provide an overall score, denoted as mean flip rate (mFP).

Baselines and Training Details. We consider several data augmentation schemes as baselines, including style transfer (Geirhos et al., 2018), AutoAugment (Cubuk et al., 2019), Mixup (Zhang et al., 2018), Manifold Mixup (Verma et al., 2019), CutMix (Yun et al., 2019), PuzzleMix (Kim et al., 2020) and AugMix (Hendrycks et al., 2020).

In our ImageNet experiments, we consider the standard ResNet-50 (He et al., 2016a) architecture as a backbone, trained on ImageNet-1k. We use publicly available models, and for a fair comparison we do not consider models that have been pretrained on larger datasets or that have been trained with any extra data to achieve better performance.

In our CIFAR-10 and CIFAR-100 experiments, we consider the preactivated ResNet-18 (He et al., 2016b) and Wide-ResNet-28x2 (Zagoruyko & Komodakis, 2016). We train all models from scratch for 200 epochs, using the same basic tuning parameters. For the augmentation schemes, we use the prescribed parameters in the corresponding papers.

4.2. ImageNet Results

Table 1 summarizes the results for ImageNet models, trained with different data augmentation schemes. Our *NoisyMix* scheme leads to a model that is substantially more robust, and it also improves the test accuracy on clean data as compared to the baseline model. In contrast, adversarial training and style transfer reduce the in-distribution test accuracy.

On ImageNet-C, *NoisyMix* gains about 13% compared to the baseline model and about 4% compared to AugMix. Since *NoisyMix* uses white noise during training, we also show the average robust accuracy in parentheses, excluding any noise perturbations (i.e., excluding white, shot and impulse noise). Table 6 in the App. provides detailed results for

each perturbation type. Further, Figure 2 shows the robust accuracy as a function of the severity level of the corruptions, and it can be seen that the advantage of our model is more pronounced with increasing severity levels.

The advantage of *NoisyMix* is also pronounced when evaluated on real-world examples as provided by the ImageNet-R dataset. This shows that *NoisyMix* not only improves the robustness with respect to synthetic distribution shifts but also to natural distribution shifts. It can also be seen that the stylized ImageNet model performs well on this task. We also use the ImageNet-R dataset to show that *NoisyMix* yields well-calibrated predictions. Table 11 in the App. shows the RMS calibration error and the area under the response rate accuracy curve (AURRA).

NoisyMix also achieves state-of-the-art result on ImageNet-P, reducing the mFP from 58% down to 28.5%. Again, we also show the mFP computed for a subset that excludes noise perturbations (i.e., white and shot noise). Table 6 in

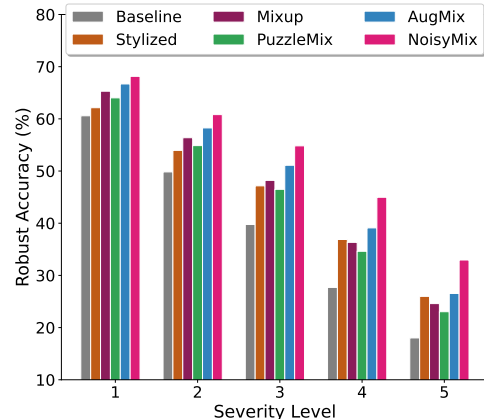


Figure 2: Robust accuracy on ImageNet-C as a function of the severity level. *NoisyMix* dominates across all levels.

Table 2: Results for ResNet-18 models trained on CIFAR-10/100 and evaluated on CIFAR-10/100-C. We train all models with 5 different seeds and show the mean and (minimum/maximum) test accuracy (higher values are better).

	CIFAR-10 ($\uparrow\%$)	CIFAR-10-C ($\uparrow\%$)	CIFAR-100 ($\uparrow\%$)	CIFAR-100-C ($\uparrow\%$)
Baseline (He et al., 2016b)	95.3 (95.2 / 95.4)	73.8 (73.5 / 74.2)	77.7 (77.5 / 78.1)	48.4 (48.0 / 48.8)
Mixup (Zhang et al., 2018)	95.8 (95.3 / 96.1)	80.4 (79.7 / 80.9)	79.7 (79.5 / 79.9)	54.2 (53.9 / 54.8)
Manifold Mixup (Verma et al., 2019)	95.9 (95.7 / 96.1)	77.7 (77.3 / 78.2)	80.3 (79.8 / 80.7)	53.4 (52.9 / 53.6)
CutMix (Yun et al., 2019)	96.5 (96.4 / 96.6)	73.0 (71.8 / 73.9)	79.3 (78.8 / 80.0)	47.9 (47.6 / 48.3)
Puzzle Mix (Kim et al., 2020)	96.5 (96.3 / 96.6)	84.1 (83.7 / 84.3)	79.4 (79.1 / 79.6)	57.4 (56.9 / 57.8)
NFM (Lim et al., 2021b)	95.4 (95.2 / 95.6)	83.3 (82.7 / 83.9)	79.4 (78.9 / 79.8)	59.7 (59.2 / 60.2)
AugMix (Hendrycks et al., 2020)	95.5 (95.0 / 95.8)	88.8 (88.1 / 89.3)	77.0 (76.6 / 77.3)	64.6 (64.4 / 64.8)
NoisyMix (ours)	95.3 (95.2 / 95.3)	91.2 (91.1 / 91.3)	79.7 (79.6 / 79.9)	71.0 (70.3 / 71.3)

Table 3: Results for Wide-ResNet-28x2 trained on CIFAR-10/100 and evaluated on CIFAR-10/100-C. We train all models with 5 different seeds and show the mean and (minimum/maximum) test accuracy (higher values are better).

	CIFAR-10 ($\uparrow\%$)	CIFAR-10-C ($\uparrow\%$)	CIFAR-100 ($\uparrow\%$)	CIFAR-100-C ($\uparrow\%$)
Baseline (Zagoruyko & Komodakis, 2016)	96.0 (95.9 / 96.1)	74.9 (74.5 / 75.4)	79.0 (78.8 / 79.1)	47.4 (47.0 / 48.0)
Mixup (Zhang et al., 2018)	96.7 (96.6 / 96.8)	80.8 (80.7 / 81.0)	80.9 (80.8 / 81.0)	53.9 (53.1 / 54.3)
Manifold Mixup (Verma et al., 2019)	96.6 (96.5 / 96.7)	77.7 (76.3 / 78.4)	81.8 (81.5 / 82.0)	53.2 (52.4 / 53.7)
CutMix (Yun et al., 2019)	96.7 (96.6 / 96.8)	71.6 (71.1 / 71.9)	80.3 (80.0 / 80.6)	48.5 (48.1 / 48.9)
Puzzle Mix (Kim et al., 2020)	97.0 (96.9 / 97.2)	82.6 (82.1 / 83.0)	81.2 (81.0 / 81.6)	56.3 (55.8 / 56.7)
NFM (Lim et al., 2021b)	96.2 (96.1 / 96.3)	82.3 (81.8 / 82.8)	80.2 (79.6 / 80.6)	58.7 (58.2 / 59.2)
AugMix (Hendrycks et al., 2020)	96.5 (96.4 / 96.6)	90.2 (89.7 / 90.7)	80.5 (79.9 / 80.8)	66.7 (65.9 / 67.2)
NoisyMix (ours)	96.3 (96.2 / 96.4)	91.8 (91.2 / 92.7)	81.3 (81.0 / 81.6)	71.9 (71.7 / 72.3)

the App. shows detailed results for all perturbation types.

To provide a complementary metric for robustness, we also evaluate the resilience of ImageNet models with respect to adversarial examples crafted by the simple fast gradient sign method (FGSM) (Goodfellow et al., 2014). *NoisyMix* helps to improve adversarial robustness with respect to these weak adversarial examples crafted with FGSM ($\epsilon = 4/255$). In contrast, AugMix is less resilient, while CutMix and PuzzleMix both show adversarial resilience.

4.3. CIFAR-10 and CIFAR-100 Results

We train ResNet-18 and Wide-ResNet-28x2 models (with 5 different seeds) on both CIFAR-10 and CIFAR-100, using different data augmentation schemes. Figure 3 shows the robust accuracy for the models evaluated on CIFAR-10-C and CIFAR-100-C. Here AugMix and *NoisyMix* show the best performance, and both schemes benefit from the use of wide architectures. In contrast, wide architectures hurt robustness when models are trained with PuzzleMix, and NFM. These results show that Wide-ResNets are not always better than ResNets, which is in agreement with recent results by Bello et al. (2021).

Table 2 and 3 provide detailed results, showing the average, minimum, and maximum test accuracy for the various test settings. Similar to the previous ImageNet results, PuzzleMix achieves the best test accuracy on clean test sets. Further, we can see that the advantage of *NoisyMix* is pro-

nounced on CIFAR-100-C, where we improve the robust accuracy by more than 5% as compared to AugMix, and this is independent of the specific architecture.

4.4. Ablation Study

At a high-level, we can decompose *NoisyMix* into 3 building blocks: (i) Noisy Feature Mixup, (ii) stability training, and (iii) data augmentations. Further, Noisy Feature Mixup can be decomposed into feature mixup and noise injections. We

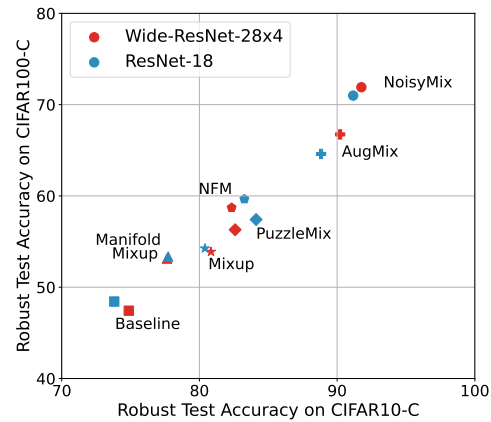


Figure 3: Robust accuracy on CIFAR-10-C and CIFAR-100-C for models trained with different data augmentation schemes. *NoisyMix* shows the best performance.

Table 4: Ablation study using a Wide-ResNet-28x2 trained on CIFAR-100. The combination of feature mixup and noise injections on top of a stability training scheme on an augmented data set boost both clean and robust accuracy.

Data Augmentations	Feature Mixup	Noise Injections	JSD Loss	CIFAR-100 ($\uparrow\%$)	CIFAR-100-C ($\uparrow\%$)	Robustness Gain (%)
\times	\times	\times	\times	79.0	47.4	-
\times	\times	\checkmark	\times	79.1	49.5	+2.1
\times	\checkmark	\times	\times	81.8	53.2	+5.8
\times	\checkmark	\checkmark	\times	80.2	58.7	+11.3
\checkmark	\times	\times	\times	79.1	64.0	+16.6
\checkmark	\times	\checkmark	\checkmark	80.9	66.7	+19.3
\checkmark	\times	\times	\checkmark	80.5	66.9	+19.5
\checkmark	\checkmark	\checkmark	\times	80.4	68.6	+21.2
\checkmark	\checkmark	\times	\checkmark	82.1	69.3	+21.9
\checkmark	\checkmark	\checkmark	\checkmark	81.3	71.9	+24.4

Table 5: Transfer learning results for ResNet-50 models trained on ImageNet and transferred to CIFAR-10/100. Then robustness is evaluated on CIFAR-10-C/100-C. Specifically, we show the average robust accuracy across all common corruptions / across noise corruptions / across whether, blur and digital corruptions.

Source Model	CIFAR-10 ($\uparrow\%$)	CIFAR-10-C ($\uparrow\%$)	CIFAR-100 ($\uparrow\%$)	CIFAR-100-C ($\uparrow\%$)
Baseline (He et al., 2016a)	97.0	77.1 / 48.8 / 86.5	84.3	57.1 / 28.0 / 66.8
PuzzleMix (Kim et al., 2020)	97.1	77.3 / 47.7 / 87.2	84.5	57.2 / 26.1 / 67.6
Mixup (Zhang et al., 2018)	97.1	78.6 / 51.7 / 87.6	84.5	57.3 / 26.4 / 67.6
AutoAugment (Cubuk et al., 2019)	97.2	78.7 / 54.6 / 86.7	84.9	57.6 / 27.3 / 67.6
AugMix (Hendrycks et al., 2020)	97.7	79.9 / 53.9 / 88.6	86.5	58.8 / 24.2 / 66.8
NoisyMix (ours)	97.7	81.8 / 60.3 / 88.9	85.9	60.3 / 34.5 / 68.8

provide a detailed ablation study to show that all components are required to achieve state-of-the-art performance.

We train models on CIFAR-100 and evaluate the in-domain test accuracy and robust accuracy on CIFAR-100-C. Table 4 shows the results, and it can be seen that data augmentations have a significant impact on robustness, i.e., robust accuracy is improved by 17%. The combination of feature mixup and noise injections helps to improve the in-domain test accuracy, while the robust accuracy is improved by about 11%. The combination of both considerably helps to improve in-domain test accuracy and robustness. The performance is further improved when stability training is used in addition, yielding our NoisyMix scheme. Indeed, NoisyMix (i.e., the favorable combination of all components) is outperforming all other variants.

4.5. Does Robustness Transfer?

Motivated by Shafahi et al. (2019b), who showed that adversarial robustness transfers, we study whether robustness to common corruptions transfers from a source model to a target task. To do so, we fine-tune ImageNet models on CIFAR-10 and CIFAR-100, and then use the corrupted test datasets to evaluate robustness.

Our results in Table 5 show that target models inherit some robustness from the source models. More robust ImageNet models, i.e., models trained with NoisyMix or Augmix, lead

to more robust target models. In particular, robustness to noise perturbations is transferred. For example, the parent model trained with NoisyMix yields target models that are about 12% more robust to noise perturbations on CIFAR-10-C and about 6% more robust on CIFAR-100-C. Moreover, a robust parent model can help to improve the in-domain accuracy on the target task, which is in alignment with the results by (Utrera et al., 2020; Salman et al., 2020).

5. Conclusion

Desirable properties of deep classifiers for computer vision are (i) in-domain accuracy, (ii) robustness to domain shifts, and (iii) well-calibrated estimation of class membership probabilities. Motivated by the challenge to achieve these, we propose NoisyMix, which combines feature mixup and noise injections with stability training on top of an augmented dataset in a single setup. Our empirical results demonstrate the advantage, i.e., improvement of (i), (ii), and (iii), when compared to standard training and other recently proposed data augmentation methods. These findings are supported by theoretical results that show that NoisyMix can improve model robustness. Future work will explore the benefits of NoisyMix beyond just computer vision tasks. In particular, we anticipate that NoisyMix will be effective in improving the robustness of models used in Scientific Machine Learning (e.g., models used for climate predictions).

Acknowledgements

N. B. Erichson and M. W. Mahoney would like to acknowledge IARPA (contract W911NF20C0035), NSF, and ONR for providing partial support of this work. S. H. Lim would like to acknowledge the WINQ Fellowship and the Knut and Alice Wallenberg Foundation for providing support of this work. Our conclusions do not necessarily reflect the position or the policy of our sponsors, and no official endorsement should be inferred. We are also grateful for the generous support from Amazon AWS.

References

- Ali, A., Dobriban, E., and Tibshirani, R. The implicit regularization of stochastic gradient flow for least squares. In *Proceedings of the International Conference on Machine Learning*, pp. 233–244. PMLR, 2020.
- An, G. The effects of adding noise during backpropagation training on a generalization performance. *Neural Computation*, 8(3):643–674, 1996.
- Bello, I., Fedus, W., Du, X., Cubuk, E. D., Srinivas, A., Lin, T.-Y., Shlens, J., and Zoph, B. Revisiting resnets: Improved training and scaling strategies. *arXiv preprint arXiv:2103.07579*, 2021.
- Bishop, C. M. Training with noise is equivalent to tikhonov regularization. *Neural Computation*, 7(1):108–116, 1995.
- Camuto, A., Willetts, M., Şimşekli, U., Roberts, S., and Holmes, C. Explicit regularisation in gaussian noise injections. *arXiv preprint arXiv:2007.07368*, 2020.
- Cubuk, E. D., Zoph, B., Mane, D., Vasudevan, V., and Le, Q. V. Autoaugment: Learning augmentation strategies from data. In *Proceedings of the Conference on Computer Vision and Pattern Recognition*, pp. 113–123, 2019.
- Deng, J., Dong, W., Socher, R., Li, L.-J., Li, K., and Fei-Fei, L. Imagenet: A large-scale hierarchical image database. In *Proceedings of the Conference on Computer Vision and Pattern Recognition*, pp. 248–255, 2009.
- DeVries, T. and Taylor, G. W. Improved regularization of convolutional neural networks with cutout. *arXiv preprint arXiv:1708.04552*, 2017.
- Dodge, S. and Karam, L. Understanding how image quality affects deep neural networks. In *Proceedings of the International Conference on Quality of Multimedia Experience*, pp. 1–6, 2016.
- Engleson, E. and Azizpour, H. Generalized Jensen-Shannon divergence loss for learning with noisy labels. *arXiv preprint arXiv:2105.04522*, 2021.
- Geirhos, R., Rubisch, P., Michaelis, C., Bethge, M., Wichmann, F. A., and Brendel, W. Imagenet-trained cnns are biased towards texture; increasing shape bias improves accuracy and robustness. In *Proceedings of the International Conference on Learning Representations*, 2018.
- Gong, C., Ren, T., Ye, M., and Liu, Q. Maxup: Lightweight adversarial training with data augmentation improves neural network training. In *Proceedings of the Conference on Computer Vision and Pattern Recognition*, pp. 2474–2483, 2021.
- Goodfellow, I., Pouget-Abadie, J., Mirza, M., Xu, B., Warde-Farley, D., Ozair, S., Courville, A., and Bengio, Y. Generative adversarial networks. *Communications of the ACM*, 63(11):139–144, 2020.
- Goodfellow, I. J., Shlens, J., and Szegedy, C. Explaining and harnessing adversarial examples. *arXiv preprint arXiv:1412.6572*, 2014.
- Gulcehre, C., Moczulski, M., Denil, M., and Bengio, Y. Noisy activation functions. In *Proceedings of the International Conference on Machine Learning*, pp. 3059–3068. PMLR, 2016.
- Guo, C., Pleiss, G., Sun, Y., and Weinberger, K. Q. On calibration of modern neural networks. In *Proceedings of the International Conference on Machine Learning*, pp. 1321–1330, 2017.
- He, K., Zhang, X., Ren, S., and Sun, J. Deep residual learning for image recognition. In *Proceedings of the Conference on Computer Vision and Pattern Recognition*, pp. 770–778, 2016a.
- He, K., Zhang, X., Ren, S., and Sun, J. Identity mappings in deep residual networks. In *Proceedings of the European Conference on Computer Vision*, pp. 630–645, 2016b.
- Hendrycks, D. and Dietterich, T. Benchmarking neural network robustness to common corruptions and perturbations. In *Proceedings of the International Conference on Learning Representations*, 2018.
- Hendrycks, D., Lee, K., and Mazeika, M. Using pre-training can improve model robustness and uncertainty. In *Proceedings of the International Conference on International Conference on Machine Learning*, pp. 2712–2721, 2019.
- Hendrycks, D., Mu, N., Cubuk, E. D., Zoph, B., Gilmer, J., and Lakshminarayanan, B. AugMix: A simple data processing method to improve robustness and uncertainty. *Proceedings of the International Conference on Learning Representations*, 2020.
- Hendrycks, D., Basart, S., Mu, N., Kadavath, S., Wang, F., Dorundo, E., Desai, R., Zhu, T., Parajuli, S., Guo, M.,

- et al. The many faces of robustness: A critical analysis of out-of-distribution generalization. In *Proceedings of the International Conference on Computer Vision*, 2021.
- Hinton, G., Vinyals, O., and Dean, J. Distilling the knowledge in a neural network. *arXiv preprint arXiv:1503.02531*, 2015.
- Kim, J.-H., Choo, W., and Song, H. O. Puzzle mix: Exploiting saliency and local statistics for optimal mixup. In *Proceedings of the International Conference on Machine Learning*, 2020.
- Krizhevsky, A. Learning multiple layers of features from tiny images. 2009.
- Krizhevsky, A., Sutskever, I., and Hinton, G. E. Imagenet classification with deep convolutional neural networks. *Proceedings of the International Conference on Neural Information Processing Systems*, 25:1097–1105, 2012.
- Kukačka, J., Golkov, V., and Cremers, D. Regularization for deep learning: A taxonomy. Technical Report Preprint: *arXiv:1710.10686*, 2017.
- Lamb, A., Verma, V., Kannala, J., and Bengio, Y. Interpolated adversarial training: Achieving robust neural networks without sacrificing too much accuracy. In *Proceedings of the 12th ACM Workshop on Artificial Intelligence and Security*, pp. 95–103, 2019.
- Lim, S. H., Erichson, N. B., Hodgkinson, L., and Mahoney, M. W. Noisy recurrent neural networks. In *Proceedings of the International Conference on Neural Information Processing Systems*, 2021a.
- Lim, S. H., Erichson, N. B., Utrera, F., Xu, W., and Mahoney, M. W. Noisy feature mixup. *arXiv preprint arXiv:2110.02180*, 2021b.
- Lin, J. Divergence measures based on the Shannon entropy. *IEEE Transactions on Information theory*, 37(1):145–151, 1991.
- Mahoney, M. W. Approximate computation and implicit regularization for very large-scale data analysis. In *Proceedings of the 31st ACM Symposium on Principles of Database Systems*, pp. 143–154, 2012.
- Rebuffi, S.-A., Goyal, S., Calian, D. A., Stimberg, F., Wiles, O., and Mann, T. Fixing data augmentation to improve adversarial robustness. *arXiv preprint arXiv:2103.01946*, 2021.
- Rice, L., Wong, E., and Kolter, Z. Overfitting in adversarially robust deep learning. In *Proceedings of the International Conference on Machine Learning*, pp. 8093–8104. PMLR, 2020.
- Rusak, E., Schott, L., Zimmermann, R. S., Bitterwolf, J., Bringmann, O., Bethge, M., and Brendel, W. A simple way to make neural networks robust against diverse image corruptions. In *Proceedings of the European Conference on Computer Vision*, pp. 53–69, 2020.
- Salman, H., Ilyas, A., Engstrom, L., Kapoor, A., and Madry, A. Do adversarially robust imagenet models transfer better? In *Proceedings of the International Conference on Neural Information Processing Systems*, volume 33, 2020.
- Shafahi, A., Najibi, M., Ghiasi, A., Xu, Z., Dickerson, J., Studer, C., Davis, L. S., Taylor, G., and Goldstein, T. Adversarial training for free! In *Proceedings of the International Conference on Neural Information Processing Systems*, 2019a.
- Shafahi, A., Saadatpanah, P., Zhu, C., Ghiasi, A., Studer, C., Jacobs, D., and Goldstein, T. Adversarially robust transfer learning. In *Proceedings of the International Conference on Learning Representations*, 2019b.
- Smith, S. L., Dherin, B., Barrett, D. G., and De, S. On the origin of implicit regularization in stochastic gradient descent. *arXiv preprint arXiv:2101.12176*, 2021.
- Szegedy, C., Zaremba, W., Sutskever, I., Bruna, J., Erhan, D., Goodfellow, I., and Fergus, R. Intriguing properties of neural networks. *arXiv preprint arXiv:1312.6199*, 2013.
- Tancik, M., Srinivasan, P. P., Mildenhall, B., Fridovich-Keil, S., Raghavan, N., Singhal, U., Ramamoorthi, R., Barron, J. T., and Ng, R. Fourier features let networks learn high frequency functions in low dimensional domains. *arXiv preprint arXiv:2006.10739*, 2020.
- Utrera, F., Kravitz, E., Erichson, N. B., Khanna, R., and Mahoney, M. W. Adversarially-trained deep nets transfer better: Illustration on image classification. In *Proceedings of the International Conference on Learning Representations*, 2020.
- Verma, V., Lamb, A., Beckham, C., Najafi, A., Mitliagkas, I., Lopez-Paz, D., and Bengio, Y. Manifold mixup: Better representations by interpolating hidden states. In *Proceedings of the International Conference on Learning Representations*, 2019.
- Weng, L. From GAN to WGAN. *arXiv preprint arXiv:1904.08994*, 2019.
- Xie, Q., Luong, M.-T., Hovy, E., and Le, Q. V. Self-training with noisy student improves imagenet classification. In *Proceedings of the Conference on Computer Vision and Pattern Recognition*, pp. 10687–10698, 2020.

- Yin, D., Gontijo Lopes, R., Shlens, J., Cubuk, E. D., and Gilmer, J. A fourier perspective on model robustness in computer vision. *Proceedings of the International Conference on Neural Information Processing Systems*, 32:13276–13286, 2019.
- Yu, B. Stability. *Bernoulli*, 19(4):1484–1500, 2013.
- Yun, S., Han, D., Oh, S. J., Chun, S., Choe, J., and Yoo, Y. Cutmix: Regularization strategy to train strong classifiers with localizable features. In *Proceedings of the International Conference on Computer Vision*, 2019.
- Zadrozny, B. and Elkan, C. Obtaining calibrated probability estimates from decision trees and naive bayesian classifiers. In *Proceedings of the International Conference on Machine Learning*, volume 1, pp. 609–616, 2001.
- Zagoruyko, S. and Komodakis, N. Wide residual networks. In *British Machine Vision Conference 2016*, 2016.
- Zhang, H., Cisse, M., Dauphin, Y. N., and Lopez-Paz, D. mixup: Beyond empirical risk minimization. In *Proceedings of the International Conference on Learning Representations*, 2018.
- Zhang, L., Deng, Z., Kawaguchi, K., Ghorbani, A., and Zou, J. How does mixup help with robustness and generalization? *arXiv preprint arXiv:2010.04819*, 2020.
- Zheng, S., Song, Y., Leung, T., and Goodfellow, I. Improving the robustness of deep neural networks via stability training. In *Proceedings of the Conference on Computer Vision and Pattern Recognition*, pp. 4480–4488, 2016.

Appendix for “NoisyMix”

In this **Appendix**, we provide additional materials to support our results in the main paper. In particular, we provide mathematical analysis of *NoisyMix* to shed light on its regularizing and robustness properties, as well as additional empirical results and the details.

Organizational Details. This **Appendix** is organized as follows.

- In Section **A**, we illustrate the regularizing effects of stability training with the JSD, Manifold Mixup, and noise injection on a toy dataset.
- In Section **B**, we study *NoisyMix* via the lens of implicit regularization. Our contributions there are Theorem 1 and Theorem 2, which show that minimizing the *NoisyMix* loss function is approximately equivalent to minimizing a sum of the original loss and data-dependent regularizers, amplifying the regularizing effects of AugMix according to the mixing and noise levels.
- In Section **C**, we show that *NoisyMix* training can improve model robustness when compared to standard training. Our main contribution there is Theorem 3, which shows that, under appropriate assumptions, *NoisyMix* training approximately minimizes an upper bound on the sum of an adversarial loss, a stability objective and data-dependent regularizers.
- In Section **D**, we provide additional experimental results and their details.

We recall the notation that we use in the main paper as well as this Appendix.

Notation. I denotes identity matrix, $[K] := \{1, \dots, K\}$, the superscript T denotes transposition, \circ denotes composition, \odot denotes Hadamard product, $\mathbb{1}$ denotes the vector with all components equal one. For a vector v , v^i denotes its i th component and $\|v\|_p$ denotes its l_p norm for $p > 0$. $M_\lambda(a, b) := \lambda a + (1 - \lambda)b$, for random variables a, b, λ . For $\alpha, \beta > 0$, $\tilde{D}_\lambda := \frac{\alpha}{\alpha+\beta} \text{Beta}(\alpha + 1, \beta) + \frac{\beta}{\alpha+\beta} \text{Beta}(\beta + 1, \alpha)$ is a uniform mixture of two Beta distributions. For the two vectors a, b , $\cos(a, b) := \langle a, b \rangle / \|a\|_2 \|b\|_2$ denotes their cosine similarity.

To simplify mathematical analysis and enable clearer intuition, we shall restrict to the special case when the mixing is done only at the input level. Moreover, we consider the setting described in the main paper for the case of $K = 2$ and $\pi_0 = \pi_1 = 1/2$ for our analysis. The results for the general case can be derived analogously using our techniques.

A. Illustration of the Regularizing Effects of Stability Training, Manifold Mixup and Noise Injection on a Toy Dataset

We consider a binary classification task for the noise corrupted 2D dataset whose points are separated by a concave polygon-shaped buffer band. Inner and outer points that disjoint the band directly correspond to two label classes, while those falling onto the band are randomly assigned to one of the classes. We generate 500 samples by setting the scale factor to be 0.5 and adding Gaussian noise with zero mean and standard deviation of 0.2 to the shape. Fig. 4 shows the data points.

We train a fully connected feedforward shallow neural network (with 32 neurons) with the ReLU activation function on these data, using 250 points for training and 250 for testing. All models are trained with Adam, learning rate of 0.1, and batch size of 50 for 100 epochs. The seed is fixed across all experiments.

We focus on the effects of stability training (with the JSD), Manifold Mixup, noise injection, and their combinations on the test performance. Note that we do not explore AugMix’s data augmentation here, since the operations used there are not meaningful for the toy dataset here.

Fig. 5 illustrates how different training schemes affect the decision boundaries of the neural network classifier. First, we can see that *NoisyMix* (which combines feature mixup, noise injections, and stability training) is most effective at smoothing the decision boundary of the trained classifiers, imposing the strongest smoothness on the dataset. Here it also yields the best test accuracy among all considered training schemes. We can also see that stability training helps to boost the effectiveness of using Manifold Mixup. In contrast, NFM without stability training performs better than the baseline and Manifold Mixup, but not as well as *NoisyMix* and Manifold Mixup with stability training.

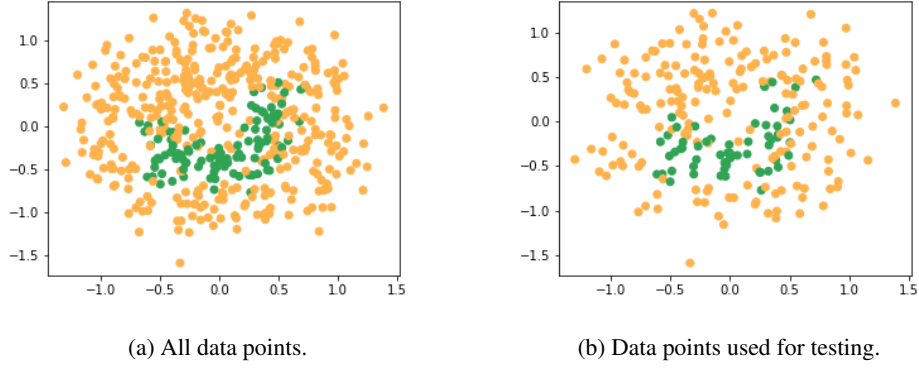


Figure 4: The dataset in \mathbb{R}^2 that we use for binary classification.

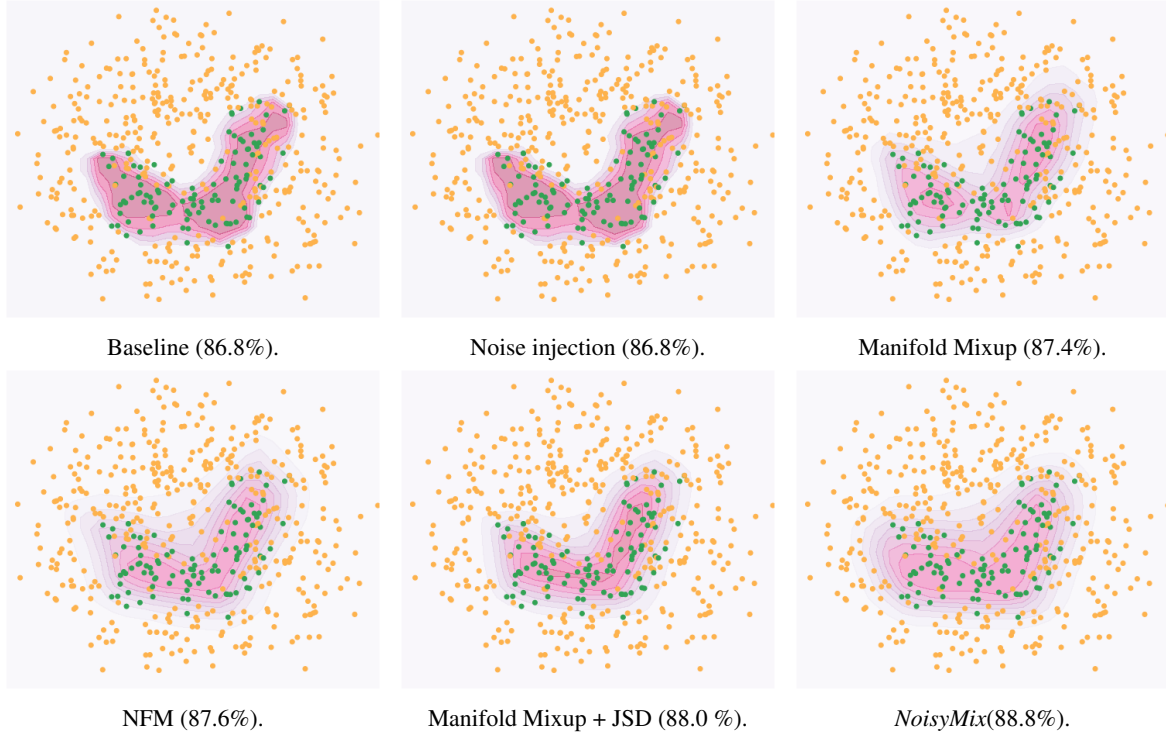


Figure 5: Decision boundaries and test accuracy (in parenthesis) for different training schemes on a 2D binary classification problem. *NoisyMix* is most effective at smoothing the decision boundary, and it also yields the best test accuracy among all considered training schemes.

B. Implicit Regularization of NoisyMix

In this section, we are going to identify the implicit regularization effects of *NoisyMix* by analyzing the NFM loss and the stability loss.

B.1. Implicit Regularization for the NFM Loss

Recall that

$$L^{NFM} = \mathbb{E}_{(x,y),(x',y') \sim \mathcal{D}} \mathbb{E}_{\lambda \sim \text{Beta}(\alpha, \beta)} \mathbb{E}_{\xi \sim \mathcal{Q}} l(p(M_{\lambda, \xi}(x, x')), M_{\lambda}(y, y')). \quad (4)$$

We consider loss functions of the form $l(p(x), y) := h(p(x)) - yp(x)$, which includes standard choices such as the logistic loss and the cross-entropy loss. Denote $L_n^{std} := \frac{1}{n} \sum_{i=1}^n l(p(x_i), y_i)$ and let \mathcal{D}_x be the empirical distribution of training samples $\{x_i\}_{i \in [n]}$. Following (Lim et al., 2021b), we shall show that NFM exhibits a natural form of implicit regularization, i.e., regularization imposed implicitly by the stochastic learning strategy or approximation algorithm, without explicitly modifying the loss.

Recall from the main paper that the NFM loss function to be minimized is

$$L_n^{NFM} = \frac{1}{n^2} \sum_{i=1}^n \sum_{j=1}^n \mathbb{E}_{\lambda \sim \text{Beta}(\alpha, \beta)} \mathbb{E}_{\xi \sim \mathcal{Q}} l(p(M_{\lambda, \xi}(x_i, x_j)), M_{\lambda}(y_i, y_j)), \quad (5)$$

where l is a loss function, $\xi := (\xi^{add}, \xi^{mult})$ are drawn from some probability distribution \mathcal{Q} with finite first two moments (with zero mean), and

$$M_{\lambda, \xi}(x, x') := (\mathbb{1} + \sigma_{mult} \xi^{mult}) \odot M_{\lambda}(x, x') + \sigma_{add} \xi^{add}. \quad (6)$$

We emphasize that this loss is computed using only the clean data.

Let $\epsilon > 0$ be a small parameter. In the sequel, we assume that l is a loss function of the form $l(p(x), y) = h(p(x)) - yp(x)$, and rescale $1 - \lambda \mapsto \epsilon(1 - \lambda)$, $\sigma_{add} \mapsto \epsilon \sigma_{add}$, $\sigma_{mult} \mapsto \epsilon \sigma_{mult}$. We recall Lemma 2 in (Lim et al., 2021b) (adapted to our setting), which will be useful later, in the following.

Lemma 1. The NFM loss (5) can be equivalently written as

$$L_n^{NFM} = \frac{1}{n} \sum_{i=1}^n \mathbb{E}_{\lambda \sim \tilde{\mathcal{D}}_{\lambda}} \mathbb{E}_{x_r \sim \mathcal{D}_x} \mathbb{E}_{\xi \sim \mathcal{Q}} [h(p(x_i + \epsilon e_i^{NFM})) - y_i p(x_i + \epsilon e_i^{NFM})], \quad (7)$$

with

$$e_i^{NFM} = (\mathbb{1} + \epsilon \sigma_{mult} \xi^{mult}) \odot e_i^{mixup} + e_i^{noise}. \quad (8)$$

Here $e_i^{mixup} = (1 - \lambda)(x_r - x_i)$ and $e_i^{noise} = \sigma_{mult} \xi^{mult} \odot x_i + \sigma_{add} \xi^{add}$, with $x_i, x_r \in \mathcal{X}$ and $\lambda \sim \text{Beta}(\alpha, \beta)$.

Note that the explicit mixing of the labels is absent in the formulation of Lemma 1. This gives a more natural interpretation of (5), in the sense that the inputs are sampled from the vicinal distribution induced by certain (data-dependent) random perturbations (see Appendix A in (Lim et al., 2021b) for more details) and the labels are kept the same.

Denote ∇p and $\nabla^2 p$ as the first and second directional derivative of p with respect to x respectively. By working in the small parameter regime, we can relate the NFM empirical loss L_n^{NFM} to the original loss L_n^{std} and identify the regularizing effects of NFM.

Theorem 1. Let $\epsilon > 0$ be a small parameter, and assume that h and p are twice differentiable. Then,

$$L_n^{NFM} = L_n^{std} + \epsilon R_1 + \epsilon^2 \tilde{R}_2 + \epsilon^2 \tilde{R}_3 + \epsilon^2 \phi(\epsilon), \quad (9)$$

with

$$\tilde{R}_2 = R_2 + \sigma_{add}^2 R_2^{add} + \sigma_{mult}^2 R_2^{mult}, \quad (10)$$

$$\tilde{R}_3 = R_3 + \sigma_{add}^2 R_3^{add} + \sigma_{mult}^2 R_3^{mult}, \quad (11)$$

where

$$R_1 = \frac{\mathbb{E}_{\lambda \sim \tilde{\mathcal{D}}_\lambda} [1 - \lambda]}{n} \sum_{i=1}^n h'(p(x_i) - y_i) \nabla p(x_i)^T \mathbb{E}_{x_r \sim \mathcal{D}_x} [x_r - x_i], \quad (12)$$

$$R_2 = \frac{\mathbb{E}_{\lambda \sim \tilde{\mathcal{D}}_\lambda} [(1 - \lambda)^2]}{2n} \sum_{i=1}^n h''(p(x_i)) \nabla p(x_i)^T \times \mathbb{E}_{x_r \sim \mathcal{D}_x} [(x_r - x_i)(x_r - x_i)^T] \nabla p(x_i), \quad (13)$$

$$R_3 = \frac{\mathbb{E}_{\lambda \sim \tilde{\mathcal{D}}_\lambda} [(1 - \lambda)^2]}{2n} \sum_{i=1}^n (h'(p(x_i)) - y_i) \times \mathbb{E}_{x_r \sim \mathcal{D}_x} [(x_r - x_i)^T \nabla^2 p(x_i) (x_r - x_i)], \quad (14)$$

$$R_2^{add} = \frac{1}{2n} \sum_{i=1}^n h''(p(x_i)) \nabla p(x_i)^T \mathbb{E}_\xi [\xi^{add} (\xi^{add})^T] \nabla p(x_i), \quad (15)$$

$$R_2^{mult} = \frac{1}{2n} \sum_{i=1}^n h''(p(x_i)) \nabla p(x_i)^T (\mathbb{E}_\xi [\xi^{mult} (\xi^{mult})^T] \odot x_i x_i^T) \nabla p(x_i), \quad (16)$$

$$R_3^{add} = \frac{1}{2n} \sum_{i=1}^n (h'(p(x_i)) - y_i) \mathbb{E}_\xi [(\xi^{add})^T \nabla^2 p(x_i) \xi^{add}], \quad (17)$$

$$R_3^{mult} = \frac{1}{2n} \sum_{i=1}^n (h'(p(x_i)) - y_i) \mathbb{E}_\xi [(\xi^{mult} \odot x_i)^T \nabla^2 p(x_i) (\xi^{mult} \odot x_i)], \quad (18)$$

and $\phi(\epsilon) = \mathbb{E}_{\lambda \sim \tilde{\mathcal{D}}_\lambda} \mathbb{E}_{x_r \sim \mathcal{D}_x} \mathbb{E}_{\xi \sim \mathcal{Q}} [\varphi(\epsilon)]$, with φ some function such that $\lim_{\epsilon \rightarrow 0} \varphi(\epsilon) = 0$.

The proof of Theorem 1 follows from a straightforward application of Theorem 1 in (Lim et al., 2021b). The key ingredients are Lemma 1 and a second-order Taylor expansion.

Theorem 1 implies that, when compared to Manifold Mixup, NFM introduces additional smoothness, regularizing the directional derivatives, $\nabla p(x_i)$ and $\nabla^2 p(x_i)$, with respect to x_i , according to the noise levels σ_{add} and σ_{mult} , and thus amplifying the regularizing effects of Manifold Mixup and noise injection. In particular, making $\nabla^2 p(x_i)$ small can lead to smooth decision boundaries (at the input level), while reducing the confidence of model predictions. On the other hand, making the $\nabla p(x_i)$ small can lead to improvement in model robustness.

B.2. Implicit Regularization for the Stability Objective

Recall that

$$L^{JSD} = \mathbb{E}_{x, x' \sim \mathcal{D}_x} \mathbb{E}_{x_{am} \sim \mathcal{A}(x), x'_{am} \sim \mathcal{A}(x')} \mathbb{E}_{\lambda \sim \text{Beta}(\alpha, \beta)} \mathbb{E}_{\xi \sim \mathcal{Q}} JS_\pi(p(M_{\lambda, \xi}(x, x')), p(M_{\lambda, \xi}(x_{am}, x'_{am}))). \quad (19)$$

The stability objective to be minimized is

$$L_n^{JSD} = \frac{1}{n^2} \sum_{i=1}^n \sum_{j=1}^n \mathbb{E}_{\lambda \sim \text{Beta}(\alpha, \beta)} \mathbb{E}_{\xi \sim \mathcal{Q}} JS_\pi(p(M_{\lambda, \xi}(x_i, x_j)), p(M_{\lambda, \xi}(A(x_i), A(x_j)))), \quad (20)$$

where $\xi := (\xi^{add}, \xi^{mult})$ are drawn from some probability distribution \mathcal{Q} with finite first two moments (with zero mean), and

$$M_{\lambda, \xi}(x, x') := (\mathbb{1} + \sigma_{mult} \xi^{mult}) \odot M_\lambda(x, x') + \sigma_{add} \xi^{add}. \quad (21)$$

Note that this loss is computed using both the clean data and the diversely transformed data.

Denote

$$\tilde{L}_n^{std} := \frac{1}{n} \sum_{i=1}^n JS_\pi(p(x_i), p(A(x_i))), \quad (22)$$

and let \mathcal{D}_x be the empirical distribution of training samples $\{x_i\}_{i \in [n]}$. We shall show that the stability objective exhibits a natural form of implicit regularization.

Let $\epsilon > 0$ be a small parameter, and rescale $1 - \lambda \mapsto \epsilon(1 - \lambda)$, $\sigma_{add} \mapsto \epsilon\sigma_{add}$, $\sigma_{mult} \mapsto \epsilon\sigma_{mult}$ as before. For this stability objective, we have the following result, derived analogously to that in Lemma 1.

Lemma 2. The JSD loss (20) can be equivalently written as

$$L_n^{JSD} = \frac{1}{n} \sum_{i=1}^n \mathbb{E}_{\lambda \sim \tilde{\mathcal{D}}_\lambda} \mathbb{E}_{x_r \sim \mathcal{D}_x} \mathbb{E}_{\xi \sim \mathcal{Q}} [JS_\pi(p(x_i + \epsilon e_i^{NFM}), p(A(x_i) + \epsilon e_i^{JSD}))], \quad (23)$$

with

$$e_i^{NFM} = (\mathbb{1} + \epsilon\sigma_{mult}\xi^{mult}) \odot e_i^{mixup} + e_i^{noise}, \quad (24)$$

and

$$e_i^{JSD} = (\mathbb{1} + \epsilon\sigma_{mult}\xi^{mult}) \odot \tilde{e}_i^{mixup} + \tilde{e}_i^{noise}. \quad (25)$$

Here $e_i^{mixup} = (1 - \lambda)(x_r - x_i)$, $e_i^{noise} = \sigma_{mult}\xi^{mult} \odot x_i + \sigma_{add}\xi^{add}$, $\tilde{e}_i^{mixup} = (1 - \lambda)(A(x_r) - A(x_i))$ and $\tilde{e}_i^{noise} = \sigma_{mult}\xi^{mult} \odot A(x_i) + \sigma_{add}\xi^{add}$, with $x_i, x_r \in \mathcal{X}$, $A \sim \mathcal{A}$ and $\lambda \sim \text{Beta}(\alpha, \beta)$.

The following proposition will be useful later.

Proposition 1. Let $\epsilon > 0$ be a small parameter. For $i = 0, 1, \dots, M$, denote $\tilde{p}_i := p(z_i + R_i(\epsilon))$, $p_i := p(z_i)$, $\nabla p_i := \nabla p(z_i)$ and $\nabla^2 p_i := \nabla^2 p(z_i)$, with the $z_i, \delta z_i \in \mathcal{X}$, and R_i some twice differentiable function such that $R_i(0) = 0$, $R'_i(0) = \delta z_i$, and $R''_i(0) = \delta^2 z_i$. Suppose that $p : \mathcal{X} \rightarrow \Delta^{K-1}$ is twice differentiable. Then, we have,

$$\begin{aligned} JS_\pi(\tilde{p}_0, \dots, \tilde{p}_M) &= JS_\pi(p_0, \dots, p_M) + \epsilon \sum_{k=1}^K \sum_{l=0}^M \pi_l \left((\nabla p_l^k)^T \delta z_l \cdot \ln \left(\frac{p_l^k}{\sum_{j=0}^M \pi_j p_j^k} \right) \right) \\ &\quad + \frac{\epsilon^2}{2} \sum_{k=1}^K \sum_{l=0}^M \pi_l \left(((\delta z_l)^T (\nabla^2 p_l^k) \delta z_l + (\nabla p_l^k)^T \delta^2 z_l) \cdot \ln \left(\frac{p_l^k}{\sum_{j=0}^M \pi_j p_j^k} \right) + \frac{((\nabla p_l^k)^T \delta z_l)^2}{p_l^k} \right) \\ &\quad - \frac{\epsilon^2}{2} \sum_{k=1}^K \frac{(\sum_{l=0}^M \pi_l (\nabla p_l^k)^T \delta z_l)^2}{\sum_{l=0}^M \pi_l p_l^k} + o(\epsilon^3), \end{aligned} \quad (26)$$

as $\epsilon \rightarrow 0$.

Proof. By definition,

$$JS_\pi(\tilde{p}_0, \dots, \tilde{p}_M) := H \left(\sum_{l=0}^M \pi_l \tilde{p}_l \right) - \sum_{l=0}^M \pi_l H(\tilde{p}_l) \quad (27)$$

$$= - \sum_{k=1}^K \left(\sum_{l=0}^M \pi_l \tilde{p}_l^k \right) \ln \left(\sum_{l=0}^M \pi_l \tilde{p}_l^k \right) + \sum_{l=0}^M \pi_l \sum_{k=1}^K \tilde{p}_l^k \ln(\tilde{p}_l^k) \quad (28)$$

$$\begin{aligned} &= - \sum_{k=1}^K \left(\sum_{l=0}^M \pi_l p^k(z_l + R_l(\epsilon)) \right) \ln \left(\sum_{l=0}^M \pi_l p^k(z_l + R_l(\epsilon)) \right) \\ &\quad + \sum_{l=0}^M \pi_l \sum_{k=1}^K p^k(z_l + R_l(\epsilon)) \ln(p^k(z_l + R_l(\epsilon))) \end{aligned} \quad (29)$$

$$= \sum_{l=0}^M \sum_{k=1}^K \pi_l A_l^k(\epsilon), \quad (30)$$

where

$$A_l^k(\epsilon) := p^k(z_l + R_l(\epsilon)) \ln \left(\frac{p^k(z_l + R_l(\epsilon))}{\sum_j \pi_j p^k(z_j + R_j(\epsilon))} \right). \quad (31)$$

Then, using twice-differentiability of p , we perform a second-order Taylor expansion on (31) in the small parameter ϵ :

$$A_l^k(\epsilon) = A_l^k(0) + \epsilon(A_l^k)'(0) + \frac{1}{2}\epsilon^2(A_l^k)''(0) + o(\epsilon^2), \quad (32)$$

as $\epsilon \rightarrow 0$.

It remains to compute $(A_l^k)'(0)$ and $(A_l^k)''(0)$.

Using chain rule, we obtain:

$$\begin{aligned} (A_l^k)'(\epsilon) &= (\nabla p^k(z_l + R_l(\epsilon)))^T R_l'(\epsilon) \left(1 + \ln \left(\frac{p^k(z_l + R_l(\epsilon))}{\sum_j \pi_j p^k(z_j + R_j(\epsilon))} \right) \right) \\ &\quad - p^k(z_l + R_l(\epsilon)) \frac{\sum_j \pi_j (\nabla p^k(z_j + R_j(\epsilon)))^T R_j'(\epsilon)}{\sum_l \pi_l p^k(z_l + R_l(\epsilon))}. \end{aligned} \quad (33)$$

Therefore, using the fact that $R_i(0) = 0$ and $R_i'(0) = \delta z_i$, we have:

$$(A_l^k)'(0) = (\nabla p^k(z_l))^T \delta z_l \left(1 + \ln \left(\frac{p^k(z_l)}{\sum_j \pi_j p^k(z_j)} \right) \right) - p^k(z_l) \frac{\sum_j \pi_j (\nabla p^k(z_j))^T \delta z_j}{\sum_l \pi_l p^k(z_l)}. \quad (34)$$

Similarly, applying chain rule, we obtain:

$$\begin{aligned} (A_l^k)''(\epsilon) &= [R_l'(\epsilon)^T \nabla^2 p^k(z_l + R_l(\epsilon)) R_l'(\epsilon) + (\nabla p^k(z_l + R_l(\epsilon)))^T R_l''(\epsilon)] \left(1 + \ln \left(\frac{p^k(z_l + R_l(\epsilon))}{\sum_j \pi_j p^k(z_j + R_j(\epsilon))} \right) \right) \\ &\quad + \frac{(\nabla p^k(z_l + R_l(\epsilon)))^T R_l'(\epsilon)^2}{p^k(z_l + R_l(\epsilon))} - \frac{2 \nabla p^k(z_l + R_l(\epsilon))^T R_l'(\epsilon) \left(\sum_j \pi_j \nabla p^k(z_j + R_j(\epsilon))^T R_j'(\epsilon) \right)}{\sum_j \pi_j p^k(z_j + R_j(\epsilon))} \\ &\quad - p^k(z_l + R_l(\epsilon)) \frac{\sum_j \pi_j (R_j'(\epsilon)^T \nabla^2 p^k(z_j + R_j(\epsilon)) R_j'(\epsilon) + \nabla p^k(z_j + R_j(\epsilon))^T R_j''(\epsilon))}{\sum_l \pi_l p^k(z_l + R_l(\epsilon))} \\ &\quad + p^k(z_l + R_l(\epsilon)) \left(\frac{\sum_l \pi_l \nabla p^k(z_l + R_l(\epsilon))^T R_l'(\epsilon)}{\sum_j \pi_j p^k(z_j + R_j(\epsilon))} \right)^2. \end{aligned} \quad (35)$$

Therefore, using the fact that $R_i(0) = 0$, $R_i'(0) = \delta z_i$, and $R_i''(0) = \delta^2 z_i$, we have:

$$\begin{aligned} (A_l^k)''(0) &= [(\delta z_l)^T \nabla^2 p^k(z_l) \delta z_l + (\nabla p^k(z_l))^T \delta^2 z_l] \left(1 + \ln \left(\frac{p^k(z_l)}{\sum_j \pi_j p^k(z_j)} \right) \right) \\ &\quad + \frac{(\nabla p^k(z_l))^T \delta z_l^2}{p^k(z_l)} - \frac{2 \nabla p^k(z_l)^T \delta z_l \left(\sum_j \pi_j \nabla p^k(z_j)^T \delta z_j \right)}{\sum_j \pi_j p^k(z_j)} \\ &\quad - p^k(z_l) \frac{\sum_j \pi_j ((\delta z_j)^T \nabla^2 p^k(z_j) \delta z_j + \nabla p^k(z_j)^T \delta^2 z_j)}{\sum_l \pi_l p^k(z_l)} \\ &\quad + p^k(z_l) \left(\frac{\sum_l \pi_l \nabla p^k(z_l)^T \delta z_j}{\sum_j \pi_j p^k(z_j)} \right)^2. \end{aligned} \quad (36)$$

Combining the above results with the Taylor expansion (32) and simplifying the resulting expression lead to (26). \square

Specializing Proposition 1 to our setting, we arrive at the following result.

Theorem 2. Let $\epsilon > 0$ be a small parameter, and assume that p is twice differentiable. Define, for $k \in [K]$,

$$q^k(x, y) := \nabla^2 p^k(x) \ln \left(\frac{2p^k(x)}{p^k(x) + p^k(y)} \right) + \nabla p^k(x) (\nabla p^k(x))^T \frac{p^k(y)}{p^k(x)(p^k(x) + p^k(y))}. \quad (37)$$

Then,

$$L_n^{JSD} = \tilde{L}_n^{std} + \epsilon S_1 + \epsilon^2 \tilde{S}_2 + \epsilon^2 \phi(\epsilon), \quad (38)$$

with

$$\tilde{S}_2 = S_2 + \sigma_{add}^2 S_2^{add} + \sigma_{mult}^2 S_2^{mult}, \quad (39)$$

where

$$S_1 = \frac{\mathbb{E}_\lambda[1 - \lambda]}{2n} \sum_{i=1}^n \sum_{k=1}^K \left((\nabla p^k(x_i))^T (\mathbb{E}_{x_r}[x_r] - x_i) \cdot \ln \left(\frac{2p^k(x_i)}{p^k(x_i) + p^k(A(x_i))} \right) \right. \\ \left. + (\nabla p^k(A(x_i)))^T (\mathbb{E}_{x_r}[A(x_r)] - A(x_i)) \cdot \ln \left(\frac{2p^k(A(x_i))}{p^k(x_i) + p^k(A(x_i))} \right) \right) \quad (40)$$

$$S_2 = \frac{\mathbb{E}_\lambda[(1 - \lambda)^2]}{4n} \sum_{i=1}^n \sum_{k=1}^K \left(\mathbb{E}_{x_r}[(x_r - x_i)^T q^k(x_i, A(x_i))(x_r - x_i)] \right. \\ \left. + \mathbb{E}_{x_r}[(A(x_r) - A(x_i))^T q^k(A(x_i), x_i)(A(x_r) - A(x_i))] \right. \\ \left. - \frac{2(\nabla p^k(x_i))^T \mathbb{E}_{x_r}[(x_r - x_i)(A(x_r) - A(x_i))^T] \nabla p^k(A(x_i))}{p^k(x_i) + p^k(A(x_i))} \right), \quad (41)$$

$$S_2^{add} = \frac{1}{4n} \sum_{i=1}^n \sum_{k=1}^K \left(\mathbb{E}_\xi[(\xi^{add})^T q^k(x_i, A(x_i))\xi^{add}] + \mathbb{E}_\xi[(\xi^{add})^T q^k(A(x_i), x_i)\xi^{add}] \right. \\ \left. - \frac{2(\nabla p^k(x_i))^T \mathbb{E}_\xi[\xi^{add}(\xi^{add})^T] \nabla p^k(A(x_i))}{p^k(x_i) + p^k(A(x_i))} \right), \quad (42)$$

$$S_2^{mult} = \frac{1}{4n} \sum_{i=1}^n \sum_{k=1}^K \left(\mathbb{E}_\xi[(\xi^{mult} \odot x_i)^T q^k(x_i, A(x_i))(\xi^{mult} \odot x_i)] \right. \\ \left. + \mathbb{E}_\xi[(\xi^{mult} \odot A(x_i))^T q^k(A(x_i), x_i)(\xi^{mult} \odot A(x_i))] \right. \\ \left. - \frac{2(\nabla p^k(x_i))^T \mathbb{E}_\xi[(\xi^{mult} \odot x_i)(\xi^{mult} \odot A(x_i))^T] \nabla p^k(A(x_i))}{p^k(x_i) + p^k(A(x_i))} \right), \quad (43)$$

and $\phi(\epsilon) = \mathbb{E}_{\lambda \sim \tilde{\mathcal{D}}_\lambda} \mathbb{E}_{x_r \sim \mathcal{D}_x} \mathbb{E}_{\xi \sim \mathcal{Q}}[\varphi(\epsilon)]$, with φ some function such that $\lim_{\epsilon \rightarrow 0} \varphi(\epsilon) = 0$.

Proof. By assumption, p is twice differentiable, so we apply Proposition 1 (with $M = 1$, $K = 2$, $\pi_0 = \pi_1 = 1/2$, $z_0 = x_i$, $z_1 = A(x_i)$, $R_0(\epsilon) = \epsilon(e_i^{mixup} + e_i^{noise}) + \epsilon^2 \sigma_{mult} \xi^{mult} \odot e_i^{mixup}$, and $R_1(\epsilon) = \epsilon(\tilde{e}_i^{mixup} + \tilde{e}_i^{noise}) + \epsilon^2 \sigma_{mult} \xi^{mult} \odot \tilde{e}_i^{mixup}$) to Eq. (23). Simplifying (using linearity of expectation, and the expression for the e_i^{mixup} , \tilde{e}_i^{mixup} , e_i^{noise} and \tilde{e}_i^{noise} given in Lemma 2) and rearranging the resulting expression then lead to the expression given in the theorem. \square

Theorem 2 implies that, when compared to the stability training in AugMix, the stability training in *NoisyMix* introduces additional smoothness, regularizing the directional derivatives, $\nabla p(x_i)$, $\nabla p(A(x_i))$, $\nabla^2 p(x_i)$ and $\nabla^2 p(A(x_i))$, with respect to both the clean data x_i and augmented data $A(x_i)$, according to the mixing coefficient and the noise levels.

Combining this with the analogous interpretation of Theorem 1 and recalling that $L_n^{NoisyMix} = L_n^{NFM} + \gamma L_n^{stability}$, we see that *NoisyMix* amplifies the regularizing effects of AugMix, and can lead to smooth decision boundaries and improvement in model robustness. Since *NoisyMix* implicitly reduces the $\nabla p(x_i)$ and $\nabla p(A(x_i))$, following the argument in Section C of (Lim et al., 2021b), we see that *NoisyMix* implicitly increases the classification margin, thereby making the model more robust to input perturbations. We shall study another lens in which *NoisyMix* can improve robustness in the next section.

C. Robustness of NoisyMix

We now demonstrate how *NoisyMix* training can lead to a model that is both adversarially robust and stable.

Following (Lamb et al., 2019; Lim et al., 2021b), we consider the binary cross-entropy loss, setting $h(z) = \log(1 + e^z)$, with the labels y taking value in $\{0, 1\}$ and the classifier model $p : \mathbb{R}^d \rightarrow \mathbb{R}$. In the following, we assume that the model parameter $\theta \in \Theta := \{\theta : y_i p(x_i) + (y_i - 1)p(x_i) \geq 0 \text{ for all } i \in [n]\}$. We remark that this set contains the set of all parameters with correct classifications of training samples (before applying *NoisyMix*), since $\{\theta : 1_{\{p(x_i) \geq 0\}} = y_i \text{ for all } i \in [n]\} \subset \Theta$. Therefore, the condition of $\theta \in \Theta$ is fulfilled when the model classifies all labels correctly for the training data before applying *NoisyMix*. Since the training error often becomes zero in finite time in practice, we shall study the effect of *NoisyMix* on model robustness in the regime of $\theta \in \Theta$.

Working in the data-dependent parameter space Θ , we obtain the following result, which is our main theoretical result.

Theorem 3. Let $\theta \in \Theta := \{\theta : y_i p(x_i) + (y_i - 1)p(x_i) \geq 0 \text{ for all } i \in [n]\}$ be a point such that $\nabla p(x_i)$, $\nabla p(A(x_i))$, $\nabla^2 p(x_i)$ and $\nabla^2 p(A(x_i))$ exist for all $i \in [n]$. Assume that $p(x_i) = \nabla p(x_i)^T x_i$, $\nabla^2 p(x_i) = 0$ for all $i \in [n]$. In addition, suppose that $\mathbb{E}_{r \sim \mathcal{D}_x}[r] = \mathbb{E}_{r \sim \mathcal{D}_x}[A(r)] = 0$ and $\|x_i\|_2 \geq c_x \sqrt{d}$ for all $i \in [n]$. Then,

$$L_n^{\text{NoisyMix}} \geq \frac{1}{n} \sum_{i=1}^n \max_{\|\delta_i\|_2 \leq \epsilon_i^{\text{mix}}} l(p(x_i + \delta_i), y_i) + \gamma \tilde{L}_n^{\text{JSD}} + \epsilon^2 L_n^{\text{reg}} + \epsilon^2 \phi(\epsilon), \quad (44)$$

where

$$\epsilon_i^{\text{mix}} = \epsilon \mathbb{E}_{\lambda \sim \tilde{\mathcal{D}}_\lambda} [1 - \lambda] \cdot c_x \sqrt{d} |\cos(\nabla p(x_i), x_i)|, \quad (45)$$

$$\tilde{L}_n^{\text{JSD}} = \frac{1 - \epsilon \mathbb{E}_{\lambda \sim \tilde{\mathcal{D}}_\lambda} [1 - \lambda]}{n} \sum_{i=1}^n \text{JS}_\pi(p(x_i), p(A(x_i))), \quad (46)$$

$$L_n^{\text{reg}} = \frac{1}{2n} \sum_{i=1}^n |h''(p(x_i))| (\epsilon_i^{\text{reg}})^2 + \gamma \tilde{S}_2, \quad (47)$$

with \tilde{S}_2 given in (39) and

$$\begin{aligned} (\epsilon_i^{\text{reg}})^2 = & \|\nabla p(x_i)\|_2^2 \left(\mathbb{E}_\lambda [(1 - \lambda)]^2 \mathbb{E}_{x_r} [\|x_r\|_2^2 \cos(\nabla p(x_i), x_r)^2] \right. \\ & + \sigma_{\text{add}}^2 \mathbb{E}_\xi [\|\xi_{\text{add}}\|_2^2 \cos(\nabla p(x_i), \xi_{\text{add}})^2] \\ & \left. + \sigma_{\text{mult}}^2 \mathbb{E}_\xi [\|\xi_{\text{mult}} \odot x_i\|_2^2 \cos(\nabla p(x_i), \xi_{\text{mult}} \odot x_i)^2] \right), \end{aligned} \quad (48)$$

and ϕ is some function such that $\lim_{\epsilon \rightarrow 0} \phi(\epsilon) = 0$.

We remark that the assumption made in Theorem 3 is similar to the one made in (Lamb et al., 2019; Zhang et al., 2020), and is satisfied by linear models and deep neural networks with ReLU activation function and max-pooling (for a proof of this, we refer to Section B.2 in (Zhang et al., 2020)).

Theorem 3 says that L_n^{NoisyMix} is approximately an upper bound of sum of an adversarial loss with l_2 -attack of size $\epsilon^{\text{mix}} = \min_i \epsilon_i^{\text{mix}}$, a stability objective, and a data-dependent regularizer. Therefore, *minimizing the NoisyMix loss would result in a small regularized adversarial loss, while promoting stability for the model*. This not only amplifies the robustness benefits of Manifold Mixup, but also imposes additional smoothness, due to the noise injection in NFM and stability training on the noise-perturbed transformed data. The latter can also help reduce robust overfitting and improve test performance (Rice et al., 2020; Rebuffi et al., 2021).

Proof of Theorem 3. The inequality in the theorem follows upon applying Theorem 2 in (Lim et al., 2021b) together with Theorem 2. \square

D. Additional Experiments and Details

In this section we show additional results to support and complement the findings in Section 4.

D.1. Additional ImageNet-C, CIFAR-10-C and CIFAR-100-C Results

ImageNet-C, CIFAR-10-C, and CIFAR-100-C consist of 15 different corruption types that are used to evaluate the robustness of a given model. These corruption types are illustrated in Figure 6. Here we show examples that corresponds to severity level 5, i.e., the most severe perturbation level. The considered corruptions cover a wide verity of perturbations that can potentially occur in real-world situations (i.e., a self-driving care might need to navigate in a snow storm).

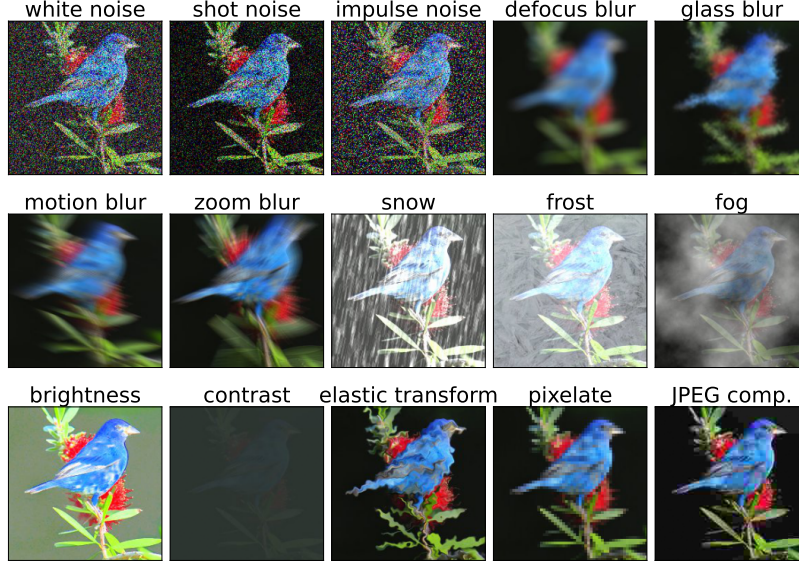


Figure 6: The ImageNet-C example shows the 15 different corruption types at severity level 5.

ImageNet-C Results. Table 6 shows the robust accuracy with respect to each perturbation type for the different ResNet-50 models trained on ImageNet-1k. *NoisyMix* performs best on 9 out of the 15 corruption types. The advantage is particularly pronounced for noise perturbations and weather corruptions. To illustrate this further, we compute the average robustness accuracy for the 4 meta categories (i.e., noise, weather, blur, and digital corruptions). The results are shown in Figure 7, where it can be seen that *NoisyMix* is the most robust model with respect to noise, weather, and digital corruptions, while AugMix is slightly more robust to blur corruptions.

Table 6: Detailed results for ResNet-50s trained with various data augmentation schemes and evaluated on ImageNet-C. All values indicate the robust accuracy (in %) as a function of the considered 15 perturbation types (higher values are better).

	Noise			Blur				Weather				Digital			
	White	Shot	Impulse	Defocus	Glass	Motion	Zoom	Snow	Frost	Fog	Bright	Contrast	Elastic	Pixel	JPEG
Baseline	29.3	27.0	23.8	38.8	26.8	38.7	36.2	32.5	38.1	45.8	68.0	39.1	45.3	44.8	53.4
Adversarial Trained	22.4	21.0	13.1	24.6	34.8	33.7	35.2	30.6	29.6	6.2	54.4	8.5	49.4	57.3	60.5
Stylized ImageNet	41.3	40.3	37.2	42.9	32.3	45.5	35.8	41.0	41.6	47.0	67.4	43.3	49.5	55.6	57.7
Fast AutoAugment	40.9	40.3	36.3	42.0	35.1	41.2	36.3	40.2	43.0	52.9	72.0	51.7	47.5	48.5	57.7
Mixup	40.5	36.9	34.2	41.9	29.1	43.9	41.1	42.0	45.5	57.5	71.4	51.0	47.1	51.8	58.6
Manifold Mixup	36.3	34.2	31.0	39.7	27.6	42.0	40.2	38.6	49.0	54.6	69.1	51.3	45.5	45.7	54.2
CutMix	36.0	34.1	28.4	40.2	25.4	40.6	36.9	34.1	39.6	50.3	70.3	46.8	45.2	36.4	51.2
Puzzle Mix	22.4	21.0	13.1	24.6	34.8	33.7	35.2	30.6	29.6	6.2	54.4	8.5	49.4	57.3	60.5
AugMix	40.6	41.1	37.7	47.7	34.9	53.5	49.0	39.9	43.8	47.1	69.5	51.1	52.0	57.0	60.3
<i>NoisyMix</i> (ours)	53.1	52.5	51.7	47.1	37.5	52.2	47.2	45.0	52.6	52.9	71.1	52.6	52.6	53.2	63.8

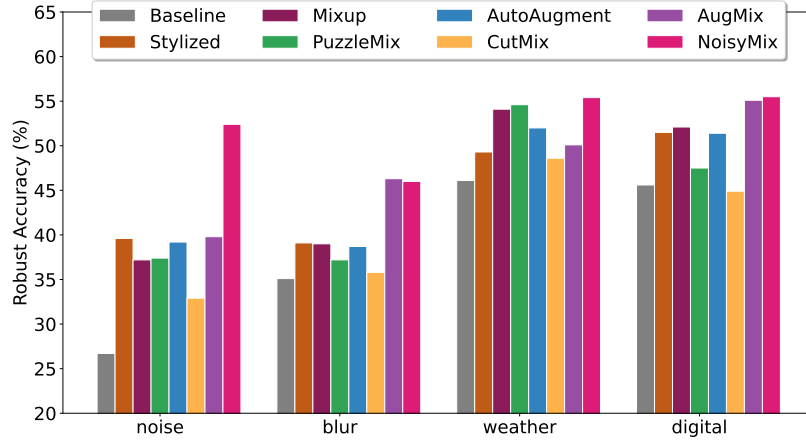


Figure 7: Average robust accuracy of ResNet-50 models for the 4 meta categories noise, blur, weather, and digital distortions. *NoisyMix* dominates in 2 out of the 4 categories, while the robustness to digital corruptions is nearly on par with AugMix.

Table 7: Detailed results for ResNet-18s trained with various data augmentation schemes and evaluated on CIFAR-10-C. All values indicate the robust accuracy (in %) as a function of the considered 15 perturbation types (higher values are better).

	Noise			Blur				Weather				Digital			
	White	Shot	Impulse	Defocus	Glass	Motion	Zoom	Snow	Frost	Fog	Bright	Contrast	Elastic	Pixel	JPEG
Baseline	46.4	59.2	52.6	82.6	53.1	78.0	77.5	82.6	78.3	88.4	93.8	76.7	84.4	74.5	79.3
Mixup	58.6	68.3	53.9	88.2	69.2	84.0	84.0	88.5	87.9	91.2	94.4	88.5	87.6	79.8	82.1
Manifold Mixup	55.5	66.4	48.2	85.7	60.5	82.3	82.5	87.3	84.9	90.7	94.5	85.1	86.2	75.3	80.9
CutMix	29.5	42.2	50.2	83.7	58.7	81.0	78.4	87.7	80.9	90.7	94.8	83.5	86.4	75.3	71.5
Puzzle Mix	76.5	81.7	69.0	86.4	77.5	83.3	82.0	90.2	90.1	91.6	95.3	87.2	88.8	85.3	77.0
NFM	78.7	83.5	73.4	85.4	72.0	80.3	83.2	89.0	89.5	87.1	94.2	76.2	86.2	82.5	87.9
AugMix	79.8	85.2	85.5	94.3	79.6	92.4	93.3	89.7	89.4	92.0	94.6	90.7	90.6	87.7	87.7
<i>NoisyMix</i> (ours)	89.9	91.8	94.6	93.6	85.9	91.6	92.7	91.1	91.7	91.1	94.5	88.1	90.9	89.3	90.7

Table 8: Detailed results for ResNet-18s trained with various data augmentation schemes and evaluated on CIFAR-100-C. All values indicate the robust accuracy (in %) as a function of the considered 15 perturbation types (higher values are better).

	Noise			Blur				Weather				Digital			
	White	Shot	Impulse	Defocus	Glass	Motion	Zoom	Snow	Frost	Fog	Bright	Contrast	Elastic	Pixel	JPEG
Baseline	22.1	30.3	24.6	60.2	21.3	54.5	53.8	54.8	48.9	64.5	73.4	55.1	60.6	51.8	50.6
Mixup	27.2	36.0	21.7	65.9	25.8	62.3	60.7	63.7	57.4	70.2	75.9	67.9	64.8	58.7	55.5
Manifold Mixup	24.7	33.6	27.0	65.1	23.1	60.8	60.3	63.8	57.3	69.2	76.7	62.8	64.6	57.2	54.2
CutMix	13.1	20.6	29.8	62.4	22.3	56.0	56.5	59.8	49.6	65.4	74.2	56.5	61.6	45.4	45.7
Puzzle Mix	47.3	54.3	40.1	64.1	33.1	59.6	59.0	64.5	59.4	68.0	75.7	60.7	64.4	56.6	54.4
NFM	50.2	57.5	42.1	64.8	34.9	59.8	61.0	66.0	64.7	65.8	76.0	57.1	65.3	64.7	64.8
AugMix	46.8	54.9	61.5	74.9	50.9	72.2	73.0	65.9	63.7	67.1	74.2	67.8	68.3	66.3	61.5
<i>NoisyMix</i> (ours)	65.3	69.2	77.8	76.8	58.6	73.7	75.4	71.1	69.7	71.0	76.7	68.0	72.2	70.5	68.9

CIFAR-C Results. Table 7 shows the detailed robustness properties of ResNet-18 models trained with different data augmentation schemes and evaluated on CIFAR-10-C. Table 8 shows similar results for ResNet-18 models that are evaluated on CIFAR-100-C. Overall, *NoisyMix* performs best across most of the different input perturbations and data corruptions as compared to various baselines in the data augmentation space. In general, the combination of a noisy training scheme paired with stability training appears to prescribe our model a bias towards stochastic noise due to the nature of fitting a reconstruction over a stochastic representation. This can be seen by the good robust accuracy on the noise, weather and digital perturbations being higher for *NoisyMix* and lower in the other methods that place less encompassing emphasis on stochastic perturbations. Overall, the advantage of training models with *NoisyMix* is more pronounced for the CIFAR-100 task, where *NoisyMix* dominates AugMix.

The limitations of certain neural network architectures in terms of their abilities to learn high-frequency features in low-

Table 9: Detailed results for Wide-ResNet models trained with data augmentation schemes and evaluated on CIFAR-10-C. All values indicate the robust accuracy (in %) as a function of the considered 15 perturbation types (higher values are better).

	Noise			Blur				Weather				Digital			
	White	Shot	Impulse	Defocus	Glass	Motion	Zoom	Snow	Frost	Fog	Bright	Contrast	Elastic	Pixel	JPEG
Baseline	46.5	59.6	50.7	83.0	57.3	79.0	78.4	85.1	81.0	89.2	94.6	77.4	85.4	76.5	79.4
Mixup	56.5	67.9	53.4	88.7	69.8	84.9	85.4	90.4	90.2	91.9	95.3	87.9	88.3	78.8	83.3
Manifold Mixup	48.0	61.1	56.4	85.7	60.1	81.6	82.3	89.0	85.9	91.4	95.4	83.3	86.4	76.3	81.7
CutMix	44.2	36.3	46.6	83.2	57.0	80.7	76.4	87.7	81.3	91.6	95.1	85.5	85.3	72.6	70.4
Puzzle Mix	72.6	79.1	58.6	85.9	72.5	83.7	80.8	91.2	89.8	92.8	95.8	89.5	88.2	82.8	75.8
NFM	74.8	81.2	71.4	84.7	69.6	78.9	81.7	89.7	89.5	88.2	95.0	73.9	86.8	81.9	87.9
AugMix	81.0	86.3	87.9	95.5	80.9	93.9	94.5	91.4	91.0	93.3	95.7	92.1	91.8	89.4	88.4
<i>NoisyMix</i> (ours)	87.0	90.2	95.7	95.3	84.2	93.4	94.4	92.3	92.2	93.4	95.8	89.8	92.5	89.5	90.8

Table 10: Detailed results for Wide-ResNet models trained with data augmentation schemes and evaluated on CIFAR-100-C. All values indicate the robust accuracy (in %) as a function of the considered 15 perturbation types (higher values are better).

	Noise			Blur				Weather				Digital			
	White	Shot	Impulse	Defocus	Glass	Motion	Zoom	Snow	Frost	Fog	Bright	Contrast	Elastic	Pixel	JPEG
Baseline	18.4	27.0	19.1	60.6	18.4	54.0	54.5	55.7	48.1	64.4	74.9	54.0	60.4	51.9	50.2
Mixup	25.3	34.3	21.0	66.5	23.6	61.8	61.3	64.5	56.1	71.1	77.1	68.2	65.4	56.3	55.8
Manifold Mixup	20.5	29.7	24.2	65.7	23.9	60.9	60.9	64.8	56.8	70.6	78.2	63.3	65.1	57.2	55.3
CutMix	13.1	20.8	31.2	62.2	22.6	57.0	55.7	61.2	52.4	67.8	75.4	59.2	61.2	43.7	44.1
Puzzle Mix	38.6	47.7	33.0	64.4	29.4	60.5	58.7	66.3	61.2	71.2	77.5	65.0	64.9	54.1	51.9
NFM	49.4	57.2	39.4	62.9	35.8	57.3	58.3	66.5	65.5	66.0	76.7	55.4	64.3	62.2	63.8
AugMix	46.6	55.5	65.2	78.2	49.3	74.8	76.1	69.0	66.1	71.5	77.6	69.9	71.2	66.9	63.2
<i>NoisyMix</i> (ours)	68.4	71.9	80.0	77.2	59.5	73.8	75.6	71.7	70.7	72.2	77.7	67.1	72.7	70.8	69.3

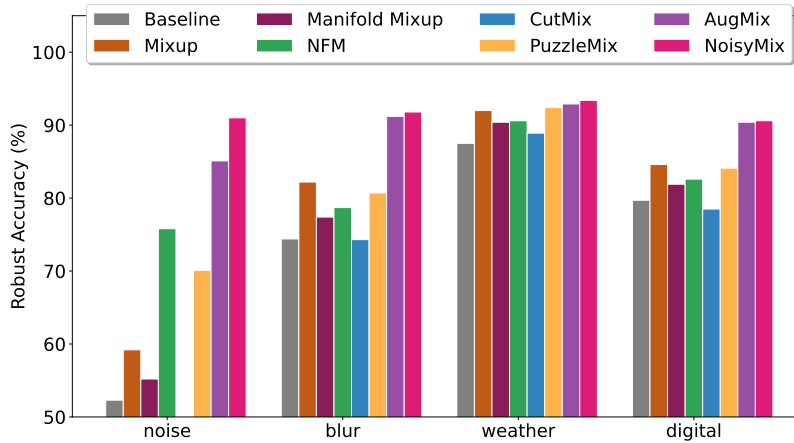


Figure 8: Average robust accuracy of Wide-ResNet-28x2 models, trained on CIFAR-10, for the 4 categories noise, blur, weather, and digital distortions. *NoisyMix* dominates in 1 out of the 4 categories, while the robustness to blur, weather, and digital corruptions is nearly on par with AugMix.

dimensional domains (Tancik et al., 2020) could also imply that our model will tend towards learning features similar in frequency to the in-domain task, and hence perform most accurately in specific out-of-domain perturbations on the same dataset containing similar frequencies. We leave this to future work.

Table 9 shows the detailed robustness properties of Wide-ResNet-28x2 models evaluated on CIFAR-10-C, and Table 10 results for CIFAR-100-C, respectively. *NoisyMix* benefits from the wide architecture and can improve the robustness as compared to the ResNet-18 models. Again, it can be seen that *NoisyMix* significantly improves the robustness to noise perturbations as well as to weather corruptions. Figure 8, and Figure 9 show the average robustness accuracy for the 4 meta categories (i.e., noise, weather, blur, and digital corruptions) for CIFAR-10-C and CIFAR-100-C, respectively.

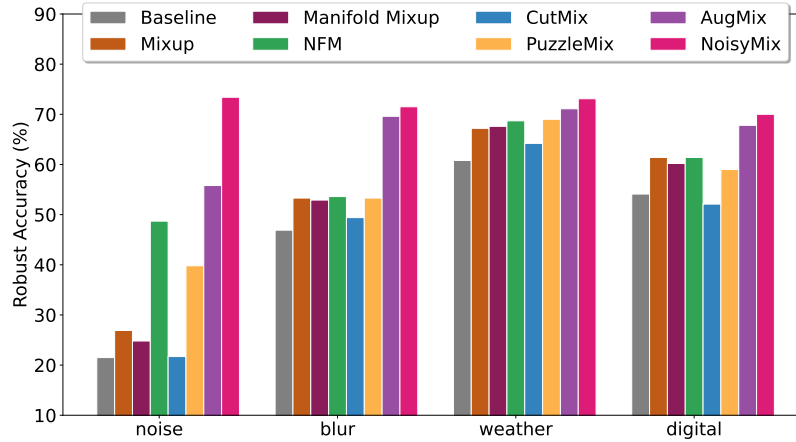


Figure 9: Average robust accuracy of Wide-ResNet-28x2 models, trained on CIFAR-100, for the 4 categories noise, blur, weather, and digital distortions. *NoisyMix* dominates in 4 out of the 4 categories.

D.2. Calibration Results for ImageNet-R

State-of-the-art neural networks tend to be biased towards high accuracy prediction, while being poorly calibrated. In turn, these models tend to be less reliable and often also show to lack fairness. This can lead to poor decision making in mission critical applications, e.g., medical imaging. In such applications it might be not sufficient to just compute a score $s(x)$ that can then be used to rank the input from the most probable member to the least probable member of a class c . Rather it is desirable to obtain a reliable estimate for the class membership probability that can be assigned an example-dependent misclassifications cost (Zadrozny & Elkan, 2001). Typically, these probability estimates are obtained by squashing the activations of the output layer through a normalized exponential function that is known as the softmax function.

One hypothesis that explains why DNNs (such as ResNets) are poorly calibrated is their high capacity, i.e., these models have the ability to learn highly-specific features that overfit to the source dataset. This phenomenon is shown by Guo et al. (2017), where calibration error increases as the number of filters per layer increases. We show that data augmentation can mitigate this effect and produce better calibrated models. Table 11 shows the RMS calibration error and the area under the response rate accuracy curve (AURRA), evaluated on ImageNet-R, as metrics to measure how well a model is calibrated. *NoisyMix* considerably improves the calibration of the ImageNet model, as compared to standard training or training with other data augmentation methods. We believe that this is explained by the fact that *NoisyMix* “wash-out” features that are highly task specific.

D.3. Additional ImageNet-P and CIFAR-10-P Results

ImageNet-C Results. Table 12 shows the flip rates with respect to each perturbation type for the different ResNet-50 models trained on ImageNet-1k. *NoisyMix* dominates on 6 out of the 10 corruption types, resulting in the lowest mean flip

Table 11: Calibration errors measured by the RMS calibration error (lower values are better), and the area under the response rate accuracy curve (higher values are better).

	RMS Calibration Error ($\downarrow\%$)	AURRA ($\uparrow\%$)
Baseline ResNet-50	19.7	64.6
Adversarial Trained (Salman et al., 2020)	8.9	68.8
Stylized ImageNet (Geirhos et al., 2018)	16.2	69.7
AutoAugment (Cubuk et al., 2019)	19.9	67.6
Mixup (Zhang et al., 2018)	17.5	68.6
Manifold Mixup (Verma et al., 2019)	5.0	68.7
CutMix (Yun et al., 2019)	13.6	63.2
Puzzle Mix (Kim et al., 2020)	15.8	68.8
AugMix (Hendrycks et al., 2020)	14.5	70.1
<i>NoisyMix</i> (ours)	3.9	74.8

Table 12: Detailed results for ResNet-50s trained with various data augmentation schemes and evaluated on ImageNet-P. The values indicate the flipping rates as a function of the 10 perturbation types (lower values are better). The mean flip rate (mFR) summarizes the results and shows that *NoisyMix* improves perturbation stability by approximately 5%.

	Noise		Blur		Weather		Digital				mFR
	White	Shot	Motion	Zoom	Snow	Bright	Translate	Rotate	Tilt	Scale	
Baseline	59.4	57.8	64.5	72.1	63.2	61.9	44.2	51.9	56.9	48.1	58.0
Adversarial Trained	25.6	40.1	26.9	33.1	18.3	60.6	25.7	31.3	30.5	40.4	33.3
Stylized ImageNet	31.1	28.8	41.8	58.1	43.1	50.3	36.7	41.2	42.9	42.1	54.4
Fast AutoAugment	53.7	49.9	63.8	79.3	66.5	58.2	43.2	49.0	57.7	43.6	56.6
Mixup	47.6	47.2	60.8	73.9	58.9	62.1	51.2	55.0	61.1	46.3	56.4
Manifold Mixup	49.1	46.2	66.1	72.4	62.6	59.9	46.5	53.7	58.8	45.2	56.0
CutMix	54.7	52.7	69.4	77.4	73.1	59.2	43.2	51.6	59.1	46.1	58.6
Puzzle Mix	50.1	48.3	64.6	72.5	63.3	56.7	44.3	50.4	57.9	46.6	55.5
AugMix	40.9	37.8	30.0	54.8	37.3	46.1	26.9	32.3	36.4	33.8	37.6
<i>NoisyMix</i> (ours)	25.1	22.8	30.2	41.5	32.4	34.1	20.5	24.5	27.7	26.3	28.5

Table 13: Detailed results for ResNet-18s trained with various data augmentation schemes and evaluated on CIFAR-10-P. The values indicate the flipping rates as a function of the 10 perturbation types (lower values are better). The mean flip rate (mFR) summarizes the results and shows that *NoisyMix* improves perturbation stability by approximately 1%.

	Noise		Blur		Weather		Digital				mFR
	White	Shot	Motion	Zoom	Snow	Bright	Translate	Rotate	Tilt	Scale	
Baseline	44.6	27.6	9.2	0.4	2.5	0.5	2.1	2.8	0.8	3.1	9.4
Mixup	26.3	17.2	6.1	0.4	1.8	0.6	2.2	2.4	0.8	2.5	6.0
Manifold Mixup	33.4	21.6	7.8	0.4	2.1	0.6	2.2	2.6	0.8	2.9	7.4
NFM	11.5	7.5	6.8	0.3	1.5	0.4	1.8	2.0	0.6	2.2	3.5
CutMix	72.3	50.8	9.1	0.5	1.9	0.6	1.9	2.3	0.8	3.1	14.3
Puzzle Mix	16.1	11.2	6.3	0.3	1.4	0.4	2.3	1.8	0.6	2.5	4.3
AugMix	11.4	7.1	2.4	0.2	1.0	0.4	1.9	1.2	0.5	1.8	2.8
<i>NoisyMix</i> (ours)	6.6	4.5	2.3	0.1	0.9	0.4	1.6	1.0	0.4	1.4	1.9

Table 14: Detailed results for Wide-ResNet-28x2 trained with various data augmentation schemes and evaluated on CIFAR-10-P. The values indicate the flipping rates as a function of the 10 perturbation types (lower values are better). The mean flip rate (mFR) summarizes the results and shows that *NoisyMix* improves perturbation stability by approximately 5%.

	Noise		Blur		Weather		Digital				mFR
	White	Shot	Motion	Zoom	Snow	Bright	Translate	Rotate	Tilt	Scale	
Baseline	42.7	27.6	8.2	0.3	2.1	0.4	1.4	2.4	0.6	2.6	8.8
Mixup	30.9	18.5	5.7	0.3	1.5	0.5	1.6	1.8	0.7	2.1	6.4
Manifold Mixup	43.8	26.6	7.0	0.3	1.6	0.4	1.3	1.9	0.6	2.2	8.6
NFM	13.1	7.8	8.0	0.3	1.4	0.4	1.4	2.0	0.6	2.1	3.7
CutMix	78.0	60.1	9.6	0.5	1.9	0.6	1.5	2.4	0.8	3.2	15.9
Puzzle Mix	14.6	9.5	7.1	0.4	1.3	0.5	1.8	1.9	0.7	2.5	4.0
AugMix	11.2	6.6	2.1	0.2	0.9	0.3	1.3	1.0	0.4	1.3	2.5
<i>NoisyMix</i> (ours)	6.3	4.2	2.0	0.1	0.7	0.3	1.0	0.8	0.3	1.1	1.7

rate overall. While *NoisyMix* shows a clear advantage compared to the model trained with AugMix, the adversarial trained model is performing nearly as good as *NoisyMix* on this task. This is surprising, since the adversarial trained model shows a poor performance on the ImageNet-C task. However, this shows the many different facets of robustness and supports the claim that there is no single metric for measuring robustness.

Table 13 and 14 show results for ResNet-18 and Wide-ResNet-28x2 models trained on CIFAR-10 and evaluated on CIFAR-10-P. Here, the models trained with *NoisyMix* clearly dominate. Note, that we do not normalize the flip rates here.